

Highlights

The Method of Harmonic Balance for the Giesekus Model under Oscillatory Shear

Shivangi Mittal, Yogesh M. Joshi, Sachin Shanbhag

- HB transforms a system of ordinary differential equations describing a dynamical system subjected to periodic perturbations into a set of nonlinear algebraic equations in frequency space.
- For the Giesekus model under large amplitude oscillatory shear, we find that harmonic balance is orders of magnitude cheaper and more accurate than the conventional method of using numerical integration to solve differential constitutive equations.

The Method of Harmonic Balance for the Giesekus Model under Oscillatory Shear

Shivangi Mittal^a, Yogesh M. Joshi^a, Sachin Shanbhag^b

^a*Department of Chemical Engineering, Indian Institute of Technology, Kanpur, 208016, Uttar Pradesh, India*

^b*Department of Scientific Computing, Florida State University, Dirac Science Library, Tallahassee, 32306, Florida, United States*

Abstract

The method of harmonic balance (HB) is a spectrally accurate method used to obtain periodic steady state solutions to dynamical systems subjected to periodic perturbations. We adapt HB to solve for the stress response of the Giesekus model under large amplitude oscillatory shear (LAOS) deformation. HB transforms the system of differential equations to a set of nonlinear algebraic equations in the Fourier coefficients. Convergence studies find that the difference between the HB and true solutions decays exponentially with the number of harmonics (H) included in the ansatz as e^{-mH} . The decay coefficient m decreases with increasing strain amplitude, and exhibits a “U” shaped dependence on applied frequency. The computational cost of HB increases slightly faster than linearly with H . The net result of rapid convergence and modest increase in computational cost with increasing H implies that HB outperforms the conventional method of using numerical integration to solve differential constitutive equations under oscillatory shear. Numerical experiments find that HB is simultaneously about three orders of magnitude cheaper, and several orders of magnitude more accurate than

numerical integration. Thus, it offers a compelling value proposition for parameter estimation or model selection.

Keywords: LAOS, spectral method, Fourier series, numerical method

1. Introduction

Rheological studies aim to understand the physics underlying a material's flow behavior, and quantify it in terms of measurable flow parameters. Stress relaxation experiments, creep tests, and oscillatory shear measurements form the backbone of this enterprise. Among these, oscillatory shear experiments allow us to probe systems over time scales that span decades without complications that arise from steep ramps and abrupt step inputs. Here, a periodic shear strain $\gamma(t) = \gamma_0 \sin(\omega t)$ with amplitude γ_0 and angular frequency ω is imposed, and the stresses generated in the material are measured.

When γ_0 is small, the resulting small amplitude oscillatory shear (SAOS) tests do not disturb the equilibrium structure, and characterize the linear response of the material. As γ_0 and ω increase, the behavior becomes increasingly nonlinear. Such large amplitude oscillatory shear (LAOS) measurements have been extensively used to study rheological phenomena including shear thinning/thickening and strain softening/hardening [1, 2, 3, 4], time-dependent structural buildup or breakage [5, 6, 7, 8, 9, 10], pseudoplasticity and elastoviscoplasticity [11, 12, 8], shear banding [13, 14, 15, 16], wall slip [17, 18, 19, 20], gelation [21, 22, 23, 24], chain stretch and entanglement in polymeric systems [25, 26, 27, 28, 29, 30], etc. Several analytical approaches have been introduced to interpret experimental LAOS data including Fourier series [31], power series [32], Pade approximants [33], Chebyshev polynomi-

als [34], stress decomposition methods [35, 36], characteristic waveforms [19], weakly nonlinear intrinsic parameters [37], sequence of physical processes [38], etc.

1.1. Representations for Oscillatory Shear Experiments

In SAOS, stress profiles becomes sinusoidal after initial transients decay. In this periodic steady (or alternance) state, the shear stress becomes [39] ,

$$\sigma_{12}^{\text{SAOS}}(t) = \gamma_0 (G'(\omega) \sin \omega t + G''(\omega) \cos \omega t) \quad (1)$$

where $G'(\omega)$ and $G''(\omega)$ are the storage and loss moduli, respectively. The corresponding normal stress differences, $N_1 = \sigma_{11} - \sigma_{22}$ and $N_2 = \sigma_{22} - \sigma_{33}$, mimic the upper convected Maxwell (UCM) model [39],

$$\begin{aligned} \frac{N_1^{\text{SAOS}}(t)}{\gamma_0^2} = G'(\omega) + & \left(G''(\omega) - \frac{G''(2\omega)}{2} \right) \sin 2\omega t + \\ & \left(-G'(\omega) + \frac{G''(2\omega)}{2} \right) \cos 2\omega t, \end{aligned} \quad (2)$$

and $N_2^{\text{SAOS}}(t) = 0$. As γ_0 and ω are increased, the steady state stresses remain periodic, but are no longer perfect sinusoids as higher harmonics are excited. Using symmetry, this nonlinear response can be represented by a Fourier series with only odd harmonics for the shear stress [40, 41],

$$\sigma_{12}(t) = \gamma_0 \sum_{\substack{n=1 \\ \text{odd}}}^{\infty} G'_n(\omega, \gamma_0) \sin n\omega t + G''_n(\omega, \gamma_0) \cos n\omega t, \quad (3)$$

where G'_n and G''_n are sine and cosine Fourier coefficients, respectively, corresponding to the n th harmonic of the shear stress. Similarly, the normal stress differences contain only even harmonics [30],

$$N_1(t) = \gamma_0^2 \sum_{\substack{n=0 \\ \text{even}}}^{\infty} F'_n(\omega, \gamma_0) \sin n\omega t + F''_n(\omega, \gamma_0) \cos n\omega t, \quad (4)$$

$$N_2(t) = \gamma_0^2 \sum_{\substack{n=0 \\ \text{even}}}^{\infty} S'_n(\omega, \gamma_0) \sin n\omega t + S''_n(\omega, \gamma_0) \cos n\omega t, \quad (5)$$

where F'_n and F''_n (S'_n and S''_n) are sine and cosine Fourier coefficients, respectively, corresponding to the n th harmonic of the first (second) normal stress difference.

In the power series representation, a further Taylor series expansion in γ_0 is performed. In the medium amplitude oscillatory shear (MAOS) or asymptotically nonlinear regime, the Taylor series is truncated after the γ_0^3 term. In this regime [32, 40, 30],

$$\begin{aligned} \sigma_{12}(t) = & \gamma_0 (G'_{11} \sin \omega t + G''_{11} \cos \omega t) + \\ & \gamma_0^3 (G'_{31} \sin \omega t + G''_{31} \cos \omega t + G'_{33} \sin 3\omega t + G''_{33} \cos 3\omega t) + \mathcal{O}(\gamma_0^5) \end{aligned} \quad (6)$$

The power series coefficients $G'_{ij}(\omega)$ and $G''_{ij}(\omega)$ are functions of only frequency, and are often called intrinsic coefficients. The coefficients $G'_{11} \equiv G'$ and $G''_{11} \equiv G''$ are identical to the linear viscoelastic moduli. The first index of the subscript (i) corresponds to the power of γ_0 , while the second index (j) corresponds to the harmonic. The Fourier coefficients are related to these power series coefficients via $G'_j = \sum_{i=j}^{\infty} \gamma_0^{i-1} G'_{ij}$ and $G''_j = \sum_{i=j}^{\infty} \gamma_0^{i-1} G''_{ij}$. Similarly, the power series representations of $N_1(t)$ and $N_2(t)$ in the MAOS regime are [30],

$$N_1(t) = F''_{00} + \gamma_0^2 (F''_{20} + F'_{22} \sin 2\omega t + F''_{22} \cos 2\omega t) + \mathcal{O}(\gamma_0^4) \quad (7)$$

$$N_2(t) = S''_{00} + \gamma_0^2 (S''_{20} + S'_{22} \sin 2\omega t + S''_{22} \cos 2\omega t) + \mathcal{O}(\gamma_0^4) \quad (8)$$

where the intrinsic coefficients F'_{ij} (S'_{ij}) and F''_{ij} (S''_{ij}) are functions of only frequency, and are analogous to G'_{ij} and G''_{ij} , respectively. A table of the symbols used in this work is provided in supplementary material.

MAOS moduli have been widely studied theoretically and experimentally. Similar to the linear viscoelastic G' and G'' , the MAOS moduli G'_{33} and G''_{33} also follow nonlinear Kramers-Kronig relations [42], which can be used to assess the validity of experimental MAOS data [43]. In the MAOS regime, the strain amplitude is barely large enough to trigger the second term of the power series but not other higher order terms. The ratio of third to first harmonic intensity is given by:

$$I_{3/1} = \frac{\sqrt{G_3'^2 + G_3''^2}}{\sqrt{G_1'^2 + G_1''^2}} \approx \gamma_0^2 \frac{\sqrt{(G_{33}')^2 + (G_{33}'')^2}}{\sqrt{(G_{11}')^2 + (G_{11}'')^2}}. \quad (9)$$

The above approximation is valid only in the MAOS regime (small γ_0) since the second term in $G_1' = G_{11}' + \gamma_0^2 G_{31}'$ vanishes as $\gamma_0 \rightarrow 0$. This leads to a quadratic dependence given by $I_{3/1} \propto \gamma_0^2$.

1.2. Constitutive Models

Constitutive models are often necessary to attribute physical meaning and interpret experimental rheological data. They consider the molecular forces generated within a material upon deformation, and yield differential or integral equations that relate stress and strain history. Numerous studies have sought to find the oscillatory shear response of different constitutive theories. Thus far, exact analytical expressions for shear and normal stresses corresponding to oscillatory strain inputs of arbitrary strain amplitude have been obtained for only two nontrivial constitutive equations: the corotational Maxwell model [44, 45], and the Oldroyd 8-constant model [46, 47]. However, both these models are quasilinear; the constitutive equations do not contain any nonlinear terms in stress.

Most analytical solutions for nonlinear constitutive equations have been obtained for only the MAOS regime, starting with early work on the Doi-Edwards theory for entangled polymer melts [48]. Indeed the list of constitutive equations with analytical expressions for the MAOS regime includes the Giesekus model [41, 15], molecular stress function theory [25], rigid rod-like polymer model [49, 50], Curtiss-Bird model [51], fourth order fluids [52], simple emulsions [53], time-strain separable Kaye-Bernstein-Kerarsley-Zapas model [54], etc. By design, these analytical expressions do not provide the full LAOS response. They are applicable only for a narrow range of γ_0 , in which γ_0 is large enough to elicit the weakest nonlinear modes, but small enough not to excite higher harmonics. In the absence of the full LAOS solution, it becomes difficult to apply these results to real systems.

The lack of analytical solutions at arbitrary strain amplitudes leaves numerical solution of the differential or integral constitutive equations as the only alternative. However, the performance of these methods degrades significantly at large γ_0 and ω . Unlike typical numerical quadrature or time-stepping algorithms, spectral methods avoid these pitfalls. For example, we recently proposed a spectral method for time-strain separable integral equations [55], which is not only more accurate than numerical quadrature, but also two to three orders of magnitude faster. It derives its speed and accuracy from a Fourier series representation of a portion of the integral equation. This combination of speed and accuracy facilitates its use in applications like Bayesian inference of model parameters [21], which requires the model to be evaluated thousands of times [56, 57]. The goal of this work is to adopt a similar technique for differential constitutive models in LAOS.

In this work, we demonstrate this approach for the Giesekus model [58], which is a popular Maxwell-type differential constitutive equation. It was originally developed for polymer solutions [59, 60, 61], where the extra stress tensor $\boldsymbol{\sigma}$,

$$\boldsymbol{\sigma} = \boldsymbol{\sigma}_p + \boldsymbol{\sigma}_s, \quad (10)$$

comprises contributions from the polymer ($\boldsymbol{\sigma}_p$), and Newtonian solvent, $\boldsymbol{\sigma}_s = \eta_s \dot{\boldsymbol{\gamma}}$, where $\dot{\boldsymbol{\gamma}}$ is the deformation tensor and η_s is solvent viscosity. Subsequently, it has been applied to wormlike micellar surfactant solutions [62, 63, 64, 65, 15], protein dispersions [66, 67], concentrated dispersions [68], etc. The polymer contribution is governed by,

$$\frac{1}{\lambda} \boldsymbol{\sigma}_p + \overset{\nabla}{\boldsymbol{\sigma}}_p + \frac{\alpha}{\lambda G} \boldsymbol{\sigma}_p \cdot \boldsymbol{\sigma}_p = G \dot{\boldsymbol{\gamma}}, \quad (11)$$

where λ and G are the relaxation time and modulus, and α is the anisotropy parameter ($0 < \alpha < 1$) that controls nonlinearity. $\overset{\nabla}{\boldsymbol{\sigma}}_p$ is the upper convected derivative defined as:

$$\overset{\nabla}{\boldsymbol{\sigma}}_p = \frac{\partial \boldsymbol{\sigma}_p}{\partial t} + \boldsymbol{v} \cdot \nabla \boldsymbol{\sigma}_p - (\nabla \boldsymbol{v})^T \cdot \boldsymbol{\sigma}_p - \boldsymbol{\sigma}_p \cdot \nabla \boldsymbol{v}, \quad (12)$$

where \boldsymbol{v} is fluid velocity. For $\alpha = 0$, the Giesekus model reduces to the UCM model with a solvent contribution, and is therefore similar to the Jeffreys model. Coupled and uncoupled multimode extensions of the Giesekus model have been successfully used for predicting complex rheological phenomena for many systems in different flow fields [69, 70, 71, 72, 73, 74].

Early studies on this model revealed its capability to capture shear thinning in a steady shear flow [59]. Holtz et al. analytically solved the response of the Giesekus model subjected to step shear strain of magnitude γ , and

verified its use for a surfactant solution [62]. The stress relaxation modulus $G(t, \gamma) = \sigma_{12}(t)/\gamma$ was found to be,

$$G(t, \gamma) = \frac{Ge^{-t/\lambda}}{1 + 2\alpha^2\gamma^2 [1 - \cosh(t/\lambda)] e^{-t/\lambda} + \alpha\gamma^2 (1 - e^{-t/\lambda})}. \quad (13)$$

Although the Giesekus model is not time-strain separable in general, it becomes separable in the long time limit ($t \rightarrow \infty$), $G(t, \gamma) = G(t)h(\gamma)$ with $h(\gamma) = (1 + \alpha(1 - \alpha)\gamma^2)^{-1}$. The weakly nonlinear response of the Giesekus model has also been investigated. Nam et al. [41] obtained analytical expressions for normal stress differences truncated beyond γ_0^2 . Ewoldt et al. proposed a Chebyshev polynomial-based method to describe the intra-cycle behavior of Giesekus model fingerprints [34]. Ewoldt and McKinley further established a mathematical and physical framework to understand self-intersections in viscous Lissajous curves for the Giesekus model under LAOS [75]. Their analysis attributed this feature to the presence of strong elastic nonlinearities that emerge in LAOS. Calin et al. proposed a method to obtain the parameters of a multimode Giesekus model from experimental SAOS and LAOS data for a semi-dilute polymer solution, using the third harmonic to obtain the anisotropy parameter α [69]. Bae and Cho proposed a semi-analytical approach for understanding MAOS response of the Giesekus model [76]. Rogers and Lettinga explained the LAOS response of the Giesekus model as a sequence of physical processes, a unique approach that is quite different from traditional Fourier analysis [38].

The linear viscoelastic response of the Giesekus model is identical to the Maxwell model; thus $G'_{11}/G = \text{De}^2/(1 + \text{De}^2)$ and $G''_{11}/G = \text{De}/(1 + \text{De}^2)$, where the Deborah number $\text{De} = \omega\lambda$. Gurnon and Wagner studied the effect of the anisotropy parameter on the stress response in LAOS and further

confirmed the presence of secondary loops in Lissajous curves even for a wormlike micellar solution [15]. They also reported the MAOS solution of the Giesekus model in terms of intrinsic power series coefficients. The intrinsic third harmonic terms for shear stress are given by,

$$\frac{G'_{31}}{G} = \frac{\alpha \text{De}^4 (-21 - 41\text{De}^2 - 8\text{De}^4 + 4\alpha (4 + 7\text{De}^2))}{4 (1 + \text{De}^2)^3 (1 + 4\text{De}^2)} \quad (14)$$

$$\frac{G''_{31}}{G} = -\frac{\alpha \text{De}^3 (9 + 11\text{De}^2 - 10\text{De}^4 + 2\alpha (-3 - \text{De}^2 + 8\text{De}^4))}{4 (1 + \text{De}^2)^3 (1 + 4\text{De}^2)} \quad (15)$$

$$\frac{G'_{33}}{G} = \frac{\alpha \text{De}^4 (-21 + 30\text{De} + 51\text{De}^4 + 4\alpha (4 - 17\text{De}^2 + 3\text{De}^4))}{4 (1 + \text{De}^2)^3 (1 + 4\text{De}^2) (1 + 9\text{De}^2)} \quad (16)$$

$$\frac{G''_{33}}{G} = \frac{\alpha \text{De}^3 (-3 + 48\text{De}^2 + 33\text{De}^4 - 18\text{De}^6 + \alpha (2 - 48\text{De}^2 + 46\text{De}^4))}{4 (1 + \text{De}^2)^3 (1 + 4\text{De}^2) (1 + 9\text{De}^2)}. \quad (17)$$

They also obtained similar expressions for the intrinsic power series coefficients of the normal stresses σ_{11} and σ_{22} corresponding to the zeroth and second harmonics [15].

1.3. Initial Value Problem and Harmonic Balance

The Giesekus model, like a majority of models for complex fluids, is expressed as a differential constitutive equation (see eqn 11). It describes a set of partial differential equations (PDEs) that can be plugged into a momentum balance equation to compute stress and flow fields for arbitrary deformations. However, in oscillatory shear experiments, the induced strain field is ideally homogeneous across the sample. In this scenario, the PDEs reduce to a set of nonlinear ordinary differential equations (ODEs), which can be posed as an initial value problem (IVP).

Typically, these nonlinear IVPs are solved numerically using a time-stepping algorithm like Runge-Kutta [77]. After initial transients decay, the solution eventually reaches a periodic limit cycle or alternance state, which is often the primary object of interest. This approach has several advantages:

- (i) **generality**: it can be easily adapted for arbitrary constitutive models,
- (ii) **software**: sophisticated algorithms for solving IVPs are already available,
- (iii) **evolution**: it tracks the evolution of the system from the initial state to the alternance state, similar to experiments.

However, it also comes with some disadvantages, especially if only the final periodic solution is of interest:

- (i) **accuracy**: stiffness of these equations especially at large γ_0 and ω can pose numerical problems, which can be addressed by using a fine time step or accepting the numerical damping that comes with a coarse step. Implicit solvers are useful in dealing with stiff ODEs, but come with additional computational cost.
- (ii) **computational cost**: in addition to the increased cost that arises from demands for greater accuracy, initial transients can take a while to decay; we cannot algorithmically speed up this process.

On the other hand, harmonic balance (HB) is a powerful technique to efficiently solve periodic dynamical systems. Such systems are encountered

across various domains of science and engineering such as transport and energy systems, acoustics, weather patterns, mechanical dampers, alternating current powered processes [78], etc. When such systems are subjected to oscillatory inputs, they eventually reach a periodic steady state. This periodic response can be expressed as a Fourier series, i.e. a linear combination of sinusoidal waveforms. This Fourier series representation or ansatz is plugged into the system of nonlinear differential equations describing the dynamics. We can determine the unknown coefficients of the Fourier series by matching or *balancing* them for each *harmonic* up to a desired level of truncation; this step gives HB its name.

Interestingly, the *numerical* technique of HB is closely related to previous efforts to *analytically* determine the MAOS response of different constitutive models. However, extending the analytical approach to higher harmonics required to describe the LAOS response is tedious, and results in unwieldy expressions. Thus, HB can be thought of as a numerical generalization of this analytical approach. In this paper, we demonstrate how HB can be used to accurately and efficiently obtain the LAOS response of the Giesekus model from first principles, by exploiting appropriate symmetries.

1.4. Layout and Scope

In this work, we establish the method of HB for solving differential constitutive relations subjected to LAOS in a computationally efficient and spectrally accurate manner by overcoming the shortcomings of conventional analytical and numerical techniques. We introduce the HB framework in section 2, and specialize it for solving the Giesekus model in LAOS. In section 3, we demonstrate the viability of the computational protocol, and study the

convergence properties of HB. Comparison with the conventional approach of numerical integration (NI) indicates that in terms of both speed and accuracy, HB is superior by orders of magnitude.

2. Methods

We begin by introducing the HB framework for a general system of ODEs. We then adapt it for the Giesekus model by exploiting symmetry constraints specific to oscillatory rheology. We review the conventional approach of NI for solving the IVP, and outline a protocol for comparing results with HB.

2.1. Harmonic Balance for Constitutive Modeling

The simplest way to introduce HB is to consider an algebraic differential equation in a single dependent variable $y(t)$,

$$f(y, \dot{y}, t) = 0, \quad (18)$$

where t is the independent variable, and $\dot{y} = dy/dt$. For a periodic output, $y(t) = y(t + T)$, where T is the period of oscillation. The Fourier series representation of $y(t)$ up to H harmonics is,

$$y(t) \approx y_H(t) = \sum_{k=-H}^H Y_k e^{ik\omega t}, \quad (19)$$

where frequency $\omega = 2\pi/T$. Here Y_k denotes the complex Fourier coefficient associated with the k th harmonic, which is defined as

$$Y_k = \frac{1}{T} \int_0^T y(t) e^{-ik\omega t} dt. \quad (20)$$

We can express the summation in equation (19) as,

$$y_H(t) = \mathbf{M}\mathbf{h}(\omega t), \quad (21)$$

where $\mathbf{M} = [Y_{-H}, \dots, Y_0, \dots, Y_H]$ is a row vector of $2H + 1$ Fourier coefficients, and $\mathbf{h}(\omega t)$ is the corresponding column vector of Fourier basis functions,

$$\mathbf{h}(\omega t) = [e^{-iH\omega t}, \dots, e^{-i\omega t}, 1, e^{i\omega t}, \dots, e^{iH\omega t}]^T \quad (22)$$

Eqn (21) effectively describes a dot product, due to the shapes of \mathbf{M} and $\mathbf{h}(\omega t)$. However, thinking of it as a matrix product is helpful with generalization to systems of equations later. Differentiating equation (19),

$$\dot{y}_H(t) = \sum_{k=-H}^H (ik\omega)Y_k e^{ik\omega t}, \quad (23)$$

we find that the Fourier coefficient of the derivative $\dot{y}_H(t)$ corresponding to k th harmonic is $(ik\omega)Y_k$. Thus, we can arrange these coefficients into a row vector with $2H+1$ elements $\dot{\mathbf{M}} = \mathbf{M}\mathbf{D}$, where $\mathbf{D} = \text{diag}(-i\omega H, \dots, 0, \dots, i\omega H)$ is a $(2H + 1) \times (2H + 1)$ diagonal matrix. This relation is instrumental in transforming differential equations in the time domain into algebraic equations in the frequency domain using Fourier transforms. When the Fourier ansatz is substituted into equation (18), we get:

$$f(y_H, \dot{y}_H, t) = r_H(t), \quad (24)$$

where we typically obtain a nonzero residual r_H , due to truncation of Fourier series after H harmonics. $r_H(t)$ inherits periodicity from $y_H(t)$, and can also be described using a Fourier series truncated after H harmonics. It can be represented by the matrix multiplication,

$$r_H(t) = \mathbf{R}\mathbf{h}(\omega t), \quad (25)$$

where \mathbf{R} is a row vector of Fourier coefficients of $r_H(t)$ with $2H + 1$ elements. Our original goal was to solve eqn (18). In HB, this is approximated by

requiring $\mathbf{R} = \mathbf{0}$. From equations (25) and (24), this is equivalent to solving $f(y_H, \dot{y}_H, t) = 0$. Note that \mathbf{R} is a function of the Fourier coefficients \mathbf{M} . Practically, setting $\mathbf{R}(\mathbf{M}) = \mathbf{0}$ involves solving a nonlinear algebraic system of $2H + 1$ unknown Fourier coefficients that are the elements of \mathbf{M} .

Generalization of HB to a system of N differential equations $\mathbf{f}(\mathbf{y}, \dot{\mathbf{y}}, t) = \mathbf{0}$ is conceptually straightforward. Here, $\mathbf{y}(t)$ and $\mathbf{y}_H(t)$ are functions of time with N components. Mathematically, equation (21) can be replaced by $\mathbf{y}_H(t) = \mathbf{M}\mathbf{h}(\omega t)$, where \mathbf{M} is now a $N \times (2H + 1)$ matrix of Fourier coefficients, with each row corresponding to one of the N components of the $\mathbf{y}_H(t)$. In this case, $\mathbf{h}(\omega t)$ remains unaltered, and is still given by eqn (22). The residual in equation (24) becomes $\mathbf{r}_H(t)$, a function of time with N components, and \mathbf{R} becomes a $N \times (2H + 1)$ matrix. The HB solution is still obtained by solving a nonlinear algebraic system,

$$\mathbf{R}(\mathbf{M}) = \mathbf{0}, \quad (26)$$

now, with $N(2H + 1)$ unknowns.

This describes the general methodology of HB. We now specialize it for differential constitutive equations in oscillatory shear, where $\mathbf{f}(\mathbf{y}, \dot{\mathbf{y}}, t) = \mathbf{0}$ typically takes the form,

$$\dot{\mathbf{y}} + \mathbf{K}\mathbf{y} + \mathbf{f}_{nl}(\mathbf{y}, t) - \mathbf{f}_{ex}(\mathbf{y}, t) = \mathbf{0}. \quad (27)$$

Here, \mathbf{K} is a $N \times N$ diagonal matrix with constant coefficients, \mathbf{f}_{nl} is a $N \times 1$ vector of nonlinear functions of the dependent variable \mathbf{y} , and \mathbf{f}_{ex} contains the external oscillatory forcing function. Substituting equation (21) into (27), and using equations (24) and (25), we obtain,

$$\mathbf{R}(\mathbf{M}) = \mathbf{M}\mathbf{D} + \mathbf{K}\mathbf{M} + \mathbf{F}_{nl}(\mathbf{M}) - \mathbf{F}_{ex}(\mathbf{M}) = \mathbf{0}, \quad (28)$$

where \mathbf{F}_{nl} and \mathbf{F}_{ex} are $N \times (2H + 1)$ matrices comprising the Fourier coefficients of the nonlinear \mathbf{f}_{nl} and external forcing functions \mathbf{f}_{ex} , respectively. $\mathbf{D} = \text{diag}(-i\omega H, \dots, 0, \dots, i\omega H)$ is the $(2H + 1) \times (2H + 1)$ diagonal matrix, alluded to earlier. This involves solving an algebraic system in $N \times (2H + 1)$ unknown elements of \mathbf{M} .

HB is most effective when both the desired solution and the residual are analytic, and can be expressed in terms of a convergent Fourier series. When a Fourier series is convergent, Fourier coefficients decay rapidly with the harmonic index H . When the system is analytic, the k th coefficient of the Fourier series decays exponentially $Y_k \sim c^{-k}$, for some constant c . In such scenarios, the difference between the ansatz solution $y_H(t)$ and the exact solution $y(t)$ decays exponentially with H [78],

$$\xi = \|y_H(t) - y(t)\|_\infty \leq u e^{-mH}, \quad (29)$$

where u and m are unknown constants, and the infinity norm $\|x\|_\infty$ denotes the maximum absolute value of $x(t)$ for $t \in [0, T]$. Thus, HB shows exponential convergence towards the true solution as H increases.

2.2. Harmonic Balance for Giesekus Model

In this work, we set solvent viscosity $\eta_s = 0$, so that $\boldsymbol{\sigma} = \boldsymbol{\sigma}_p$, and the subscript ‘ p ’ can be dropped. For homogeneous flow, the single-mode Giesekus model described by eqns (10) and (11) can be expressed as a set of nonlinear

ODEs,

$$\begin{aligned}
\frac{d\sigma_{11}}{dt} + \frac{\sigma_{11}}{\lambda} + \frac{\alpha}{\lambda G} (\sigma_{11}^2 + \sigma_{12}^2) - 2\dot{\gamma}\sigma_{12} &= 0 \\
\frac{d\sigma_{22}}{dt} + \frac{\sigma_{22}}{\lambda} + \frac{\alpha}{\lambda G} (\sigma_{22}^2 + \sigma_{12}^2) &= 0 \\
\frac{d\sigma_{33}}{dt} + \frac{\sigma_{33}}{\lambda} + \frac{\alpha}{\lambda G} \sigma_{33}^2 &= 0 \\
\frac{d\sigma_{12}}{dt} + \frac{\sigma_{12}}{\lambda} + \frac{\alpha}{\lambda G} (\sigma_{11} + \sigma_{22}) \sigma_{12} - \sigma_{22}\dot{\gamma} - G\dot{\gamma} &= 0.
\end{aligned} \tag{30}$$

Here, $\dot{\gamma}(t) = \gamma_0\omega \cos \omega t$ is the oscillatory shear rate, and α, λ , and G are system parameters. Since the evolution of σ_{33} does not depend on other components of the stress tensor $\boldsymbol{\sigma}$, we can set the steady state $\sigma_{33} = 0$, and retain only $N = 3$ dynamic variables, $\mathbf{y} = [\sigma_{11}, \sigma_{22}, \sigma_{12}]^T$. Thus, equation (30) can be cast in the form of equation (27) with a 3×3 diagonal matrix $\mathbf{K} = \lambda^{-1}\mathbf{I}$, where \mathbf{I} is the identity matrix. Then \mathbf{f}_{nl} contains all the quadratic nonlinear terms,

$$\mathbf{f}_{nl} = \frac{\alpha}{\lambda G} \begin{bmatrix} (\sigma_{11}^2 + \sigma_{12}^2) \\ (\sigma_{22}^2 + \sigma_{12}^2) \\ (\sigma_{11} + \sigma_{22})\sigma_{12} \end{bmatrix}, \tag{31}$$

and \mathbf{f}_{ex} consists of forcing terms with $\dot{\gamma} = \gamma_0\omega \cos(\omega t) = \frac{\gamma_0\omega}{2} (e^{i\omega t} + e^{-i\omega t})$,

$$\mathbf{f}_{ex} = \frac{\gamma_0\omega}{2} (e^{i\omega t} + e^{-i\omega t}) \begin{bmatrix} 2\sigma_{12} \\ 0 \\ (G + \sigma_{22}) \end{bmatrix}. \tag{32}$$

This system can be transformed to the Fourier domain, and solved using HB according to equations (21) – (28). Using arguments of symmetry, the shear and normal stresses can be represented as truncated Fourier series with only odd and even harmonics, respectively. This reduces the number of unknown coefficients by nearly half.

Consider a Fourier series with H odd harmonics in shear stress. We adopt a convention in which $(2H - 1)\omega$ and $(2H - 2)\omega$ are the highest harmonics present in shear and normal stresses, respectively. Note that it is possible to choose a convention where $2H$ is the highest harmonic present in the normal stresses. For small values of γ_0 in the linear viscoelastic regime, this choice is optimal since $H = 1$ is sufficient to describe the second harmonic that is excited in N_1 and N_2 . On the other hand, the MAOS response is typically represented by truncating the power series representation beyond the third harmonic (see eqns 6 – 8), in which case the convention we adopt is optimal since $H = 2$ is sufficient. Regardless, the objective of this work is to explore the LAOS regime which calls for modestly large values of H . In such scenarios, the specific convention adopted becomes unimportant. Using our convention, the shear and normal stresses are written as,

$$\begin{aligned}
\sigma_{11}(t) &= \sum_{k=-(H-1)}^{H-1} A_{2k} e^{i2k\omega t} \\
\sigma_{22}(t) &= \sum_{k=-(H-1)}^{H-1} B_{2k} e^{i2k\omega t} \\
\sigma_{12}(t) &= \sum_{k=-H}^{H-1} C_{2k+1} e^{i(2k+1)\omega t}.
\end{aligned} \tag{33}$$

There are $2H - 1$ Fourier coefficients corresponding to the first and second normal stresses. Similarly there are $2H$ Fourier coefficients corresponding to the shear stress. Let

$$\mathbf{M} = [\{A_{2k}\}_{k=-(H-1)}^{H-1}, \{B_{2k}\}_{k=-(H-1)}^{H-1}, \{C_{2k+1}\}_{k=-H}^{H-1}] \tag{34}$$

be the vector of unknown coefficients. The total number of elements in \mathbf{M} is $(6H - 2)$. In principle, these Fourier coefficients are complex, and the

total number of unknowns is twice as many. However, since stresses are real, Fourier coefficients are complex conjugates; for example, $A_{2k} = \bar{A}_{-2k}$, where the overbar is used to denote the conjugate. This means that the real and imaginary parts are related as $\text{Re}(A_{2k}) = \text{Re}(\bar{A}_{-2k})$, and $\text{Im}(A_{2k}) = -\text{Im}(\bar{A}_{-2k})$.

We can substitute eqn (33) into eqn (30), and truncate the quadratic nonlinear term after the highest harmonic ($2H - 1$) is resolved. For step-by-step derivation of the following equations (eqns (35) – (37)) please refer to the supplementary material. For the ODE involving σ_{11} , we obtain a set of $2H - 1$ algebraic nonlinear equations in the Fourier coefficients for $k \in [-(H - 1), H - 1]$,

$$R_k^{11}(\mathbf{M}) = \frac{\alpha}{\lambda G} \left(\sum_{m=-(H-1)}^{H-1} A_{2m} A_{2(k-m)} + \sum_{m=-H}^{H-1} C_{2m+1} C_{2(k-m)-1} \right) + \left(i2k\omega + \frac{1}{\lambda} \right) A_{2k} - \gamma_0 \omega (C_{2k-1} + C_{2k+1}) = 0. \quad (35)$$

Here and subsequently, all harmonics higher than those prescribed by the ansatz are assumed to be zero. Thus, $A_j = B_j = 0$ for $|j| > 2H - 2$ and $C_j = 0$ for $|j| > 2H - 1$. The quadratic nonlinearity of the Giesekus model is reflected in the quadratic terms multiplying the factor $\alpha/\lambda G$. These quadratic terms are multiplications of two Fourier series and can be determined using the convolution theorem [78]. The ODE involving σ_{22} also reduces to a set of $2H - 1$ quadratic equations for $k \in [-(H - 1), H - 1]$,

$$R_k^{22}(\mathbf{M}) = \frac{\alpha}{\lambda G} \left(\sum_{m=-(H-1)}^{H-1} B_{2m} B_{2(k-m)} + \sum_{m=-H}^{H-1} C_{2m+1} C_{2(k-m)-1} \right) + \left(i2k\omega + \frac{1}{\lambda} \right) B_{2k} = 0. \quad (36)$$

Finally, the ODE for σ_{12} leads to $2H$ equations for $k \in [-H, H - 1]$

$$R_k^{12}(\mathbf{M}) = \left(i(2k + 1)\omega + \frac{1}{\lambda} \right) C_{2k+1} + \frac{\alpha}{\lambda G} \sum_{m=-H}^{H-1} C_{2m+1} (A_{2(k-m)} + B_{2(k-m)}) - \gamma_0 \omega \left(\frac{B_{2k} + B_{2k+2}}{2} \right) - \frac{G\gamma_0 \omega}{2} \delta_{|2k+1|1} = 0, \quad (37)$$

where $\delta_{|2k+1|1}$ in the last term of this equation is a Kronecker delta function that is nonzero only when $k = -1$ or $k = 0$. This term arises from the externally applied shear force, in which only the first harmonic is triggered.

The residuals corresponding to the equations (35) – (37) are stacked into an array,

$$\mathbf{R}(\mathbf{M}) = [\{R_k^{11}(\mathbf{M})\}_{k=-(H-1)}^{H-1}, \{R_k^{22}(\mathbf{M})\}_{k=-(H-1)}^{H-1}, \{R_k^{12}(\mathbf{M})\}_{k=-H}^{H-1}] \quad (38)$$

with $6H - 2$ elements. We can thus solve these nonlinear equations for \mathbf{M} by using a suitable nonlinear solver that seeks to minimize the residuals. Once we obtain the solution \mathbf{M} , and therefore all the Fourier coefficients, we can compute the dynamic moduli used in the Fourier representation, eqns (3) – (5), via, $G'_n = i(C_n - C_{-n})$, $G''_n = (C_n + C_{-n})$, $F'_n = i((A_n - B_n) - (A_{-n} - B_{-n}))$, $F''_n = ((A_n - B_n) + (A_{-n} - B_{-n}))$, $S'_n = i(B_n - B_{-n})$, and $S''_n = (B_n + B_{-n})$.

2.3. Solving Harmonic Balance Equations

HB leads to a system of nonlinear equations in $6H - 2$ unknowns stacked in the vector \mathbf{M} (eqn. (34)), which can be expressed in terms of the $6H - 2$ elements of the residual vector \mathbf{R} (eqn. (38)). We solve these equations using the MATLAB function `fsolve`. It uses a trust region dogleg algorithm, which belongs to a popular class of methods for optimization problems. It attempts

to solve for the elements of \mathbf{M} by minimizing the elements of the residual \mathbf{R} . We set the termination criterion as $\|\mathbf{R}\|_\infty < 10^{-12}$.

In this work, the LAOS response of the Giesekus model is computed at different frequencies ω , and three decades of strain amplitude γ_0 spanning the range $10^{-2} - 10^1$. The input to `fsolve` is the residual vector $\mathbf{R}(\mathbf{M})$ as a function of the unknown coefficients \mathbf{M} , and an initial estimate of the solution vector. For small strains, $\gamma_0 \lesssim 0.1$, we use the analytical MAOS response as the initial guess [15]. All Fourier coefficients corresponding to harmonics greater than the third harmonic are set to zero. This is a reasonably good initial guess for small strains. This is important because nonlinear systems can have multiple solutions, some of which may even be unstable. A good initial guess mitigates the risk of converging to unstable solutions, as `fsolve` typically converges to the solution closest to it.

As γ_0 increases beyond 0.1, the solution gradually begins to deviate from the MAOS response. Hence, we use a ladder approach to develop good initial guesses for intermediate and large values of γ_0 . In this work, the ladder comprises three intermediate rungs at strain amplitudes given by [1.0, 2.2, 4.6] that are dispersed between 0.1 and 10. Thus, we selected $\gamma_0 = 0.1$ and $\gamma_0 = 1$ as the first two steps of this ladder, and two intermediate rungs between $\gamma_0 = 1 - 10$, that are logarithmically equispaced. For any given value of γ_0 between 0.1 - 10, say $\gamma_0 = 3.5$, we first use the analytical MAOS solution as an initial estimate for the response at $\gamma_0 = 0.1$. We then use the HB solution obtained at $\gamma_0 = 0.1$ as the initial guess for the γ_0 corresponding to the next rung in the ladder, which is $\gamma_0 = 1$. This process is repeated until the value of γ_0 at which the solution is desired is smaller than the γ_0 that corresponds

to the next rung of the ladder. By staging the solution in this manner, we ensure that a good initial guess is available for the solver. This gradually activates higher harmonics as γ_0 is increased, and avoids convergence to incorrect solution branches, especially at high frequencies.

2.4. Solving IVP

To solve the IVP, we first recast the ODEs in eqn (30) in dimensionless form. If we do not non-dimensionalize the ODEs, the numerical solution becomes unstable at large ω and γ_0 . Using $\tilde{t} = t/\lambda$, $\tilde{\sigma} = \sigma/(G\lambda\omega\gamma_0)$, $\tilde{\gamma} = \dot{\gamma}/(\gamma_0\omega) = \cos(\text{De}\tilde{t})$, $\text{De} = \lambda\omega$, and Wiessenberg number $\text{Wi} = \lambda\gamma_0\omega$ [79], we obtain,

$$\begin{aligned} r_{11}(\tilde{t}) &= \frac{d\tilde{\sigma}_{11}}{d\tilde{t}} + \tilde{\sigma}_{11} + \alpha\text{Wi}(\tilde{\sigma}_{11}^2 + \tilde{\sigma}_{12}^2) - 2\tilde{\gamma}\tilde{\sigma}_{12}\text{Wi} \approx 0 \\ r_{22}(\tilde{t}) &= \frac{d\tilde{\sigma}_{22}}{d\tilde{t}} + \tilde{\sigma}_{22} + \alpha\text{Wi}(\tilde{\sigma}_{22}^2 + \tilde{\sigma}_{12}^2) \approx 0 \\ r_{12}(\tilde{t}) &= \frac{d\tilde{\sigma}_{12}}{d\tilde{t}} + \tilde{\sigma}_{12} + \alpha\text{Wi}(\tilde{\sigma}_{11} + \tilde{\sigma}_{22})\tilde{\sigma}_{12} - \tilde{\gamma} - \tilde{\gamma}\tilde{\sigma}_{22}\text{Wi} \approx 0 \end{aligned} \quad (39)$$

The residuals $r_{11}(\tilde{t})$, $r_{22}(\tilde{t})$, and $r_{12}(\tilde{t})$ should ideally be zero if the exact solution is inserted in the above equations. However, numerical approximation results in nonzero residuals, which are nevertheless themselves periodic.

We solve the ODEs given by eqn (39) using the adaptive implicit Runge-Kutta method `ode23s` in MATLAB. In order to obtain the alternance solution, we monitor the relative difference between successive peaks of the stress outputs. This difference falls as the initial transients decay, and eventually becomes equal to zero. Once the relative difference falls below a suitable threshold (10^{-6} in this work), we assume that the periodic steady state has been attained. The number of oscillation cycles or time required to reach

steady state depends on the magnitude of γ_0 and ω . Once the periodic steady state solution is obtained, it is interpolated at $N_t = 1000$ uniformly spaced grid points per cycle using cubic splines. Fourier representations of the numerically computed stresses are obtained using fast Fourier transform (FFT). This allows us to write,

$$\tilde{\boldsymbol{\sigma}}_{\text{IVP}}(\tilde{t}) = \begin{bmatrix} \tilde{\sigma}_{11} \\ \tilde{\sigma}_{22} \\ \tilde{\sigma}_{12} \end{bmatrix} = \frac{1}{G\text{Wi}} \begin{bmatrix} \sum_n \gamma_0^2 (P'_n \sin n \text{De} \tilde{t} + P''_n \cos n \text{De} \tilde{t}) \\ \sum_n \gamma_0^2 (Q'_n \sin n \text{De} \tilde{t} + Q''_n \cos n \text{De} \tilde{t}) \\ \sum_n \gamma_0 (G'_n \sin n \text{De} \tilde{t} + G''_n \cos n \text{De} \tilde{t}) \end{bmatrix}, \quad (40)$$

where the summation over n extends to the largest nonzero mode, and includes only even and odd harmonics for normal and shear stresses, respectively. The normal stress coefficients P'_n and P''_n (and Q'_n and Q''_n) are analogous to G'_n and G''_n for the shear stress. They can be used to obtain the coefficients corresponding to the first and second normal stress differences,

$$\begin{aligned} F'_n &= P'_n - Q'_n, & F''_n &= P''_n - Q''_n, \\ S'_n &= Q'_n, & S''_n &= Q''_n. \end{aligned} \quad (41)$$

2.5. Comparing HB and NI solutions

How can we compare the accuracy of the solution obtained using HB and NI, especially in the LAOS regime, where the exact solution is not known? One approach, and the one we adopt here, is to compare the magnitude of the residual or error obtained by inserting the numerical solution back into the set of ODEs. We describe how to compute this error term, first for NI, and then for HB.

Once the numerical solution $\tilde{\boldsymbol{\sigma}}_{\text{IVP}}(\tilde{t})$ is obtained in the form shown in equation (40), we can symbolically compute the derivative at any arbitrary

time as,

$$\frac{d\tilde{\boldsymbol{\sigma}}_{\text{IVP}}}{d\tilde{t}} = \frac{1}{GWi} \begin{bmatrix} \sum_n nDe\gamma_0^2 (P'_n \cos(nDe\tilde{t}) - P''_n \sin(nDe\tilde{t})) \\ \sum_n nDe\gamma_0^2 (Q'_n \cos(nDe\tilde{t}) - Q''_n \sin(nDe\tilde{t})) \\ \sum_n nDe\gamma_0 (G'_n \cos(nDe\tilde{t}) - G''_n \sin(nDe\tilde{t})) \end{bmatrix}, \quad (42)$$

where the summation over n runs over indices identical to equation (40). We can substitute equations (40) and (42) in the dimensionless ODEs (eqn (39)), and compute the residuals $r_{11}(\tilde{t})$, $r_{22}(\tilde{t})$, and $r_{12}(\tilde{t})$.

To compare solutions over a period of oscillation, we divide a single dimensionless period $\tilde{T} = 2\pi/De$ into $N_t = 1000$ uniformly spaced points $\tilde{t}_i = i\Delta\tilde{t}$ for $i = 0, \dots, N_t - 1$, with $\Delta\tilde{t} = \tilde{T}/N_t$. Residuals are evaluated at these points, and stacked into a vector, $\boldsymbol{r} = [r_{11}(\tilde{t}_i), r_{22}(\tilde{t}_i), r_{12}(\tilde{t}_i)]_{i=0}^{N_t-1}$ with $3N_t$ elements. The error associated with this term can be computed from the root mean square value of \boldsymbol{r} via the Euclidean or 2-norm as,

$$\epsilon_r = \frac{1}{3N_t} \|\boldsymbol{r}\|_2. \quad (43)$$

We can follow a nearly identical process to compute ϵ_r from the HB solution $\boldsymbol{\sigma}_{\text{HB}}$ which is obtained in a form given by eqn (33). We then (i) non-dimensionalize this solution similar to eqn (40), (ii) symbolically compute the first derivative of eqn (33) using (42), (iii) insert these expressions in the dimensionless ODEs eqn (39), (iv) compute the residual vector \boldsymbol{r} at the same points $\{\tilde{t}_i\}$, and (v) evaluate the error ϵ_r .

3. Results and Discussion

We examine results for the oscillatory shear response of the Giesekus model obtained using HB. In all the calculations performed in this study,

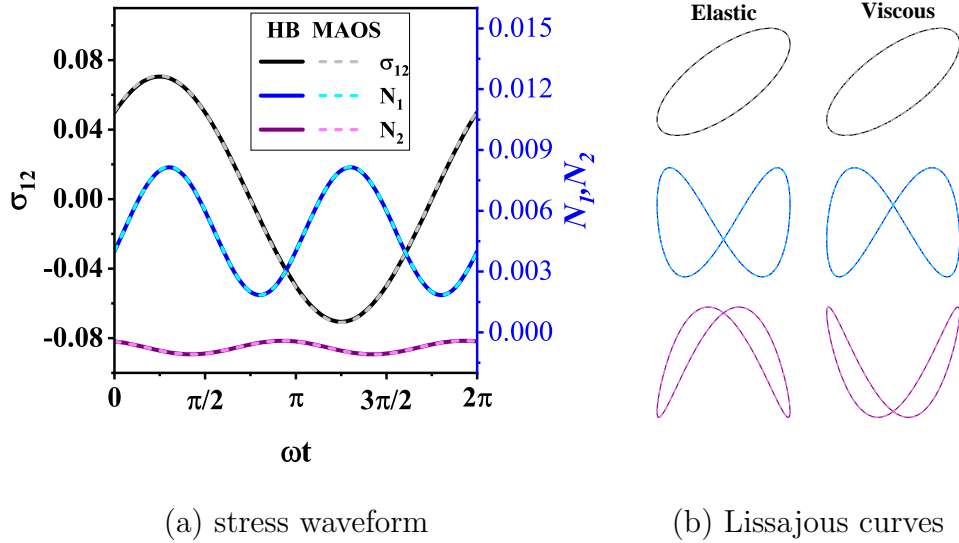
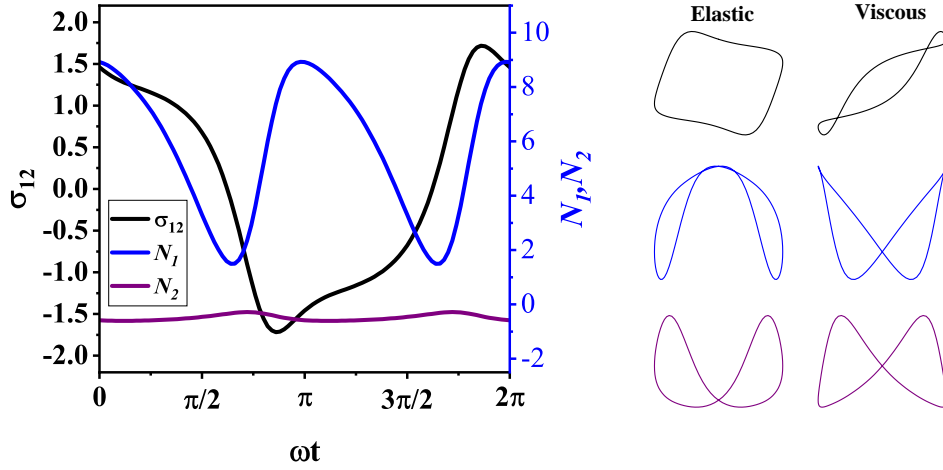


Figure 1: The stress response of the Giesekus model at $\gamma_0 = 0.1$ and $De = 1$ computed with HB method (solid lines) overlaps the MAOS analytical solution (dashed lines) for the (a) shear and normal stress waveforms, and (b) the corresponding elastic and viscous Lissajous curves.

we assume $G = 1$ Pa, $\lambda = 1$ s, $\alpha = 0.3$ and $\eta_s = 0$ Pa·s. We analyze the periodic stress waveforms and harmonic coefficients over a range of γ_0 and ω . We study the convergence rate as the number of harmonics in the ansatz is increased. Finally, we compare HB and NI in terms of accuracy and computational cost.

3.1. Stress waveforms and Lissajous plots

We begin by comparing the computed oscillatory stress response using HB with known analytical solutions in the weakly nonlinear or MAOS regime with $\gamma_0 = 0.1$, and $\omega = 1$ rad/s. In the HB method, we set $H = 5$. The resulting periodic stress waveforms for σ_{12} , N_1 , and N_2 are shown in figure



(a) stress waveform

(b) Lissajous curves

Figure 2: The oscillatory stress response of the Giesekus model at $\gamma_0 = 10$ and $De = 1$ computed with HB method. The computed (a) shear and normal stress waveforms, and the corresponding (b) elastic and viscous Lissajous curves are shown, similar to figure 1.

1(a). The waveforms are approximately sinusoidal, and do not exhibit the effect of strong nonlinearities. The corresponding normalized elastic and viscous Lissajous curves are shown in figure 1(b). The elastic Lissajous curves plot the stress versus strain normalized by their maximum values. For the shear stress, this shows $\sigma_{12}(t)/\sigma_{12}^{\max}$ versus $\gamma(t)/\gamma_0 = \sin \omega t$, where σ_{12}^{\max} corresponds to the magnitude of the maximum value of $\sigma_{12}(t)$ in figure 1(a). Similarly, the viscous Lissajous curves plot the stress versus strain rate, normalized by their maximum values. For $\gamma_0 = 0.1$, the peak magnitude of σ_{12} is greater than the peak magnitude of N_1 and N_2 . N_2 is smaller than N_1 , and is negative. The analytical MAOS solution for the shear and normal stress differences is overlaid on both plots using dashed lines, and essentially overlaps with the computed solution.

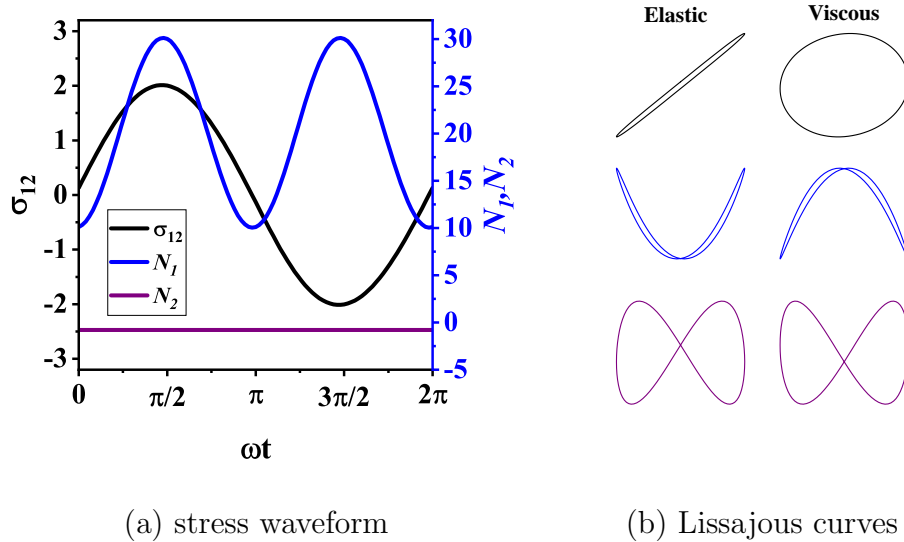


Figure 3: The oscillatory stress response of the Giesekus model at $\gamma_0 = 10$ and $De = 100$ computed with HB method. The computed (a) shear and normal stress waveforms, and the corresponding (b) elastic and viscous Lissajous curves are shown, similar to figure 1.

Figure 2 shows results similar to figure 1 at a frequency of $\omega = 1$ rad/s, but at a higher strain amplitude of $\gamma_0 = 10$. This corresponds to $De = 1$ and $Wi = 10$, and strongly activates the nonlinear terms in the model. The stress waveforms are significantly distorted, and far from sinusoidal. The peak magnitude of N_1 becomes significantly larger than the peak magnitudes of σ_{12} and N_2 . Mathematically, the combination of moderate De and large Wi leads to a tightly coupled system which is manifested in the emergence of secondary loops in the Lissajous curves. The occurrence of self-intersections in Lissajous curves has been reported for many experimental systems [80, 34, 81, 11, 82, 83, 84, 85], and constitutive models [80, 86, 87], including the Giesekus model [75, 15].

Secondary loops disappear at large frequency $\omega = 100$ rad/s as shown in figure 3. Here $\gamma_0 = 10$, similar to figure 2. Despite the large $De = 100$ and $Wi = 1000$, the stress waveform shown in 3(a) is not distorted, and the Lissajous curves no longer exhibit self-intersections associated with a strong viscoelastic response. Elasticity dominates material response at such high frequencies resulting in surprisingly simple profiles.

Figure 4 plots the intensities of the harmonics for shear and normal stress differences corresponding to the three cases studied in figures 1 – 3. For shear stress, the intensity of the k th harmonic is defined as $I_k = \sqrt{(G'_k)^2 + (G''_k)^2}$. Analogous expressions are used for normal stress differences. In figure 4, these intensities are normalized by the leading harmonic i.e., I_1 for shear stress, and I_0 for normal stress differences. These plots quantitatively reinforce our qualitative observations from the stress waveforms and Lissajous curves. In figure 4(a), the weakness of harmonics beyond the first for the shear stress, and beyond the second for normal stresses, suggests that linear viscoelastic modes still dominate the response. On the other hand, higher harmonics exhibit slow decay in figure 4(b) due to the tight coupling in Giesekus model equations, with I_3/I_1 being 23% and I_4/I_0 being 14%. The contribution of higher harmonics is small in figure 4(c), despite being deep in the LAOS regime, due to the dominance of elastic contributions. Thus, a strong deformation does not guarantee the activation of larger modes and hence, a judicious choice of H is necessary to ensure convergence of the HB method while minimizing the computational effort.

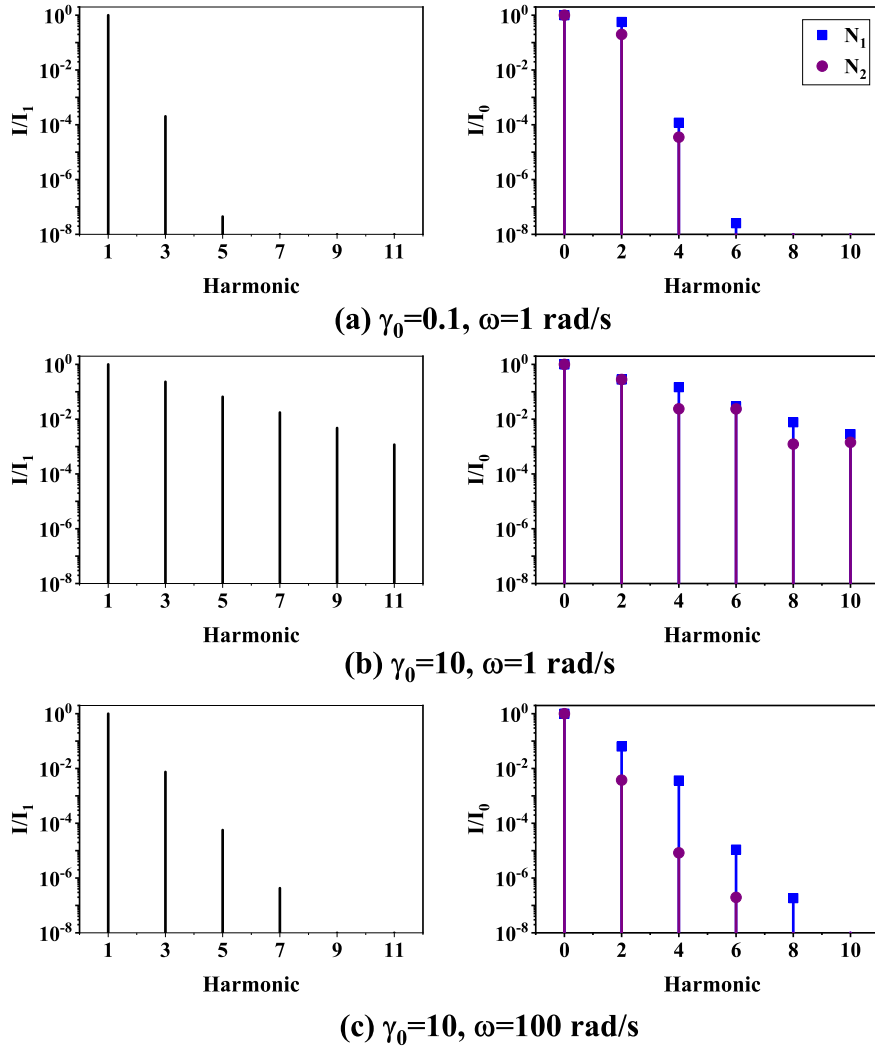


Figure 4: Normalized harmonic intensities for shear stress I/I_1 (left column), and normal stress difference I/I_0 (right column) at (a) $\gamma_0 = 0.1, \omega = 1$ rad/s, (b) $\gamma_0 = 10, \omega = 1$ rad/s, and (c) $\gamma_0 = 10, \omega = 100$ rad/s using HB.

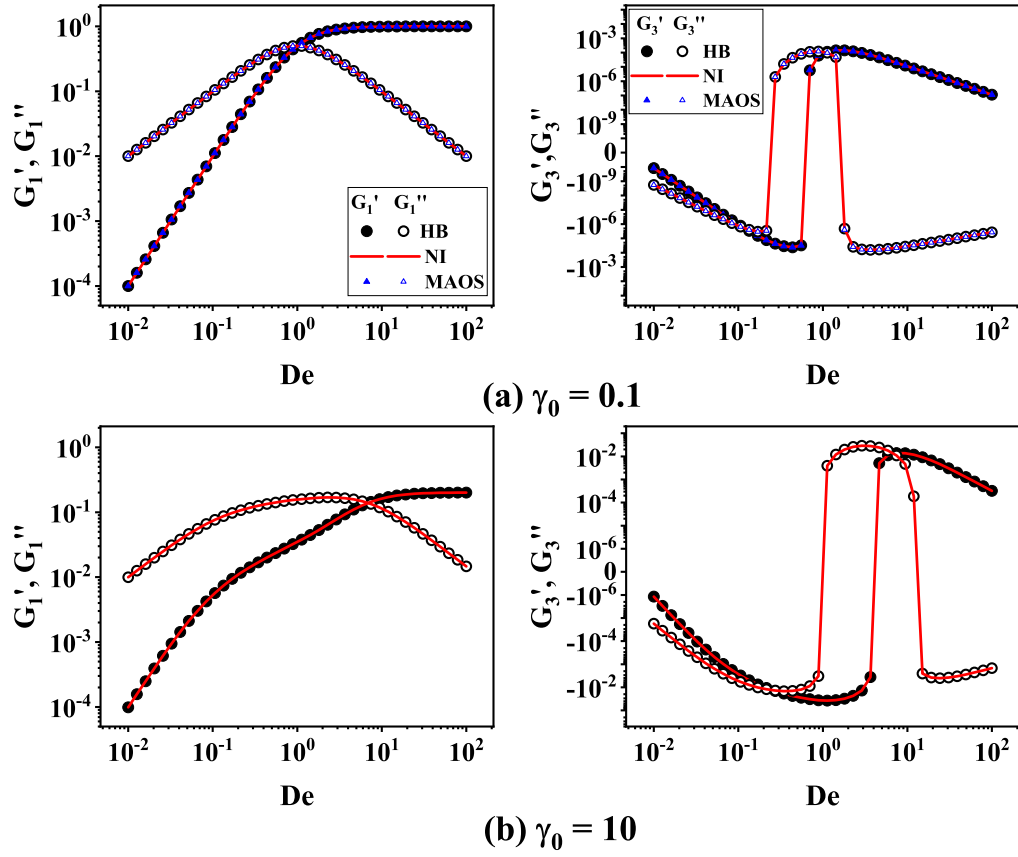


Figure 5: The Fourier coefficients of shear stress (G'_1, G''_1, G'_3 , and G''_3) at (a) $\gamma_0 = 0.1$ and (b) $\gamma_0 = 10$ using HB, and NI. The analytical MAOS solution shown in subfigure (a) overlaps with the HB solution.

3.2. Frequency Sweeps of Leading Nonlinear Harmonics

Figure 5 shows the first and third harmonic coefficients for shear stress at $\gamma_0 = 0.1$ and $\gamma_0 = 10$ across four decades of frequency, $\omega \in [10^{-2}, 10^2]$. For the HB solution, storage moduli are shown by filled circles, while loss moduli are shown by open circles. The analytical MAOS solution is shown by small triangles [15]. The third harmonic takes both positive and negative values. Hence, we use a symmetrical logscale (or symlog) to represent the vertical axis. In these plots, a small linear region is introduced near the origin to account for sign changes. The HB solution is in good agreement with the analytical MAOS solutions.

The nonlinear regime in oscillatory shear can be crudely defined by $De > 1$ and $Wi > 1$. Figure 5 shows the expected increase in relative intensity of the third harmonic and decrease in the magnitude of primary harmonics as we move towards the LAOS regime. The third harmonic becomes more than 10% of the first harmonic at $\gamma_0 = 10$ which leads to a distorted stress waveform and secondary loops in viscous Lissajous-Bowditch curves in the range of $0.1 < De < 3$, as discussed previously.

Figure 6 and 7 represent the corresponding coefficients for the first normal stress difference and second normal stress difference, respectively, over four decades of frequency at $\gamma_0 = 0.1$ and $\gamma_0 = 10$. The normal stress coefficients are found by normalizing the harmonics with γ_0^2 . Notice that the leading order terms for N_1 and N_2 are always positive and negative respectively. Similar to our observations for the shear stress coefficients, the magnitude of primary harmonics (0ω and 2ω terms) decline as the contributions of higher frequencies become significant at larger γ_0 . In addition, the frequencies at

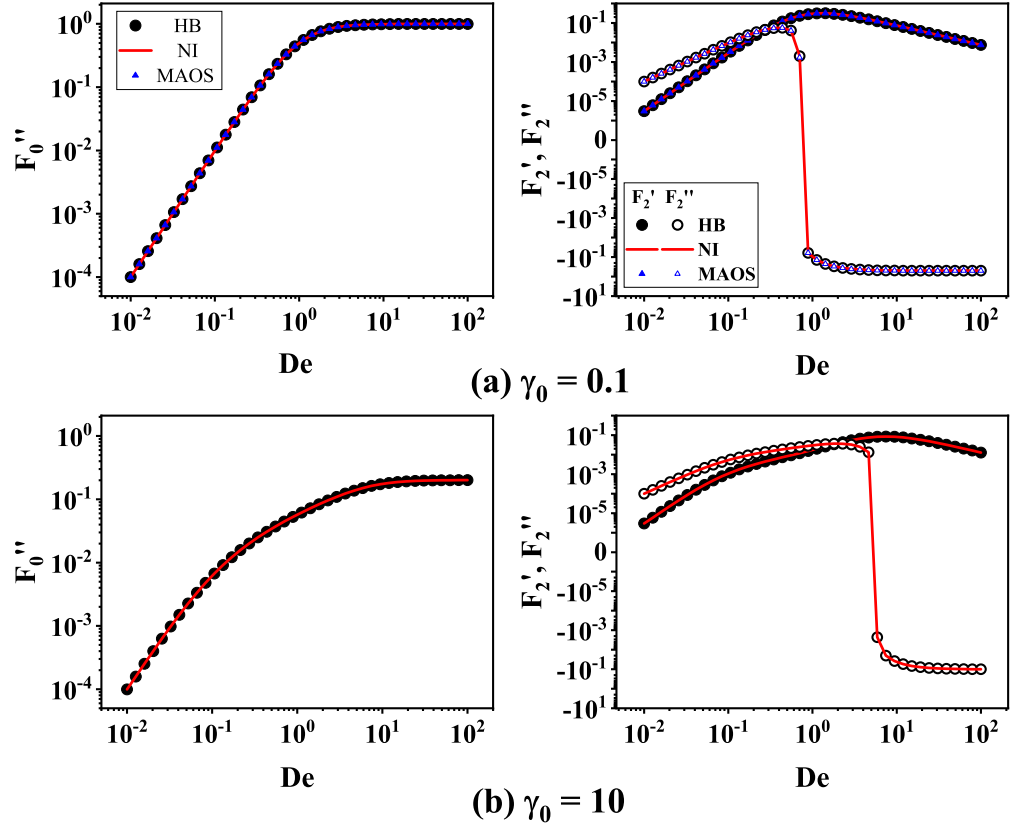


Figure 6: The Fourier coefficients of the first normal stress difference (F_0'' , F_2' and F_2'') at (a) $\gamma_0 = 0.1$, and (b) $\gamma_0 = 10$ using harmonic balance (HB), and numerical integration (NI). The analytical MAOS solution is shown in subfigure (a).

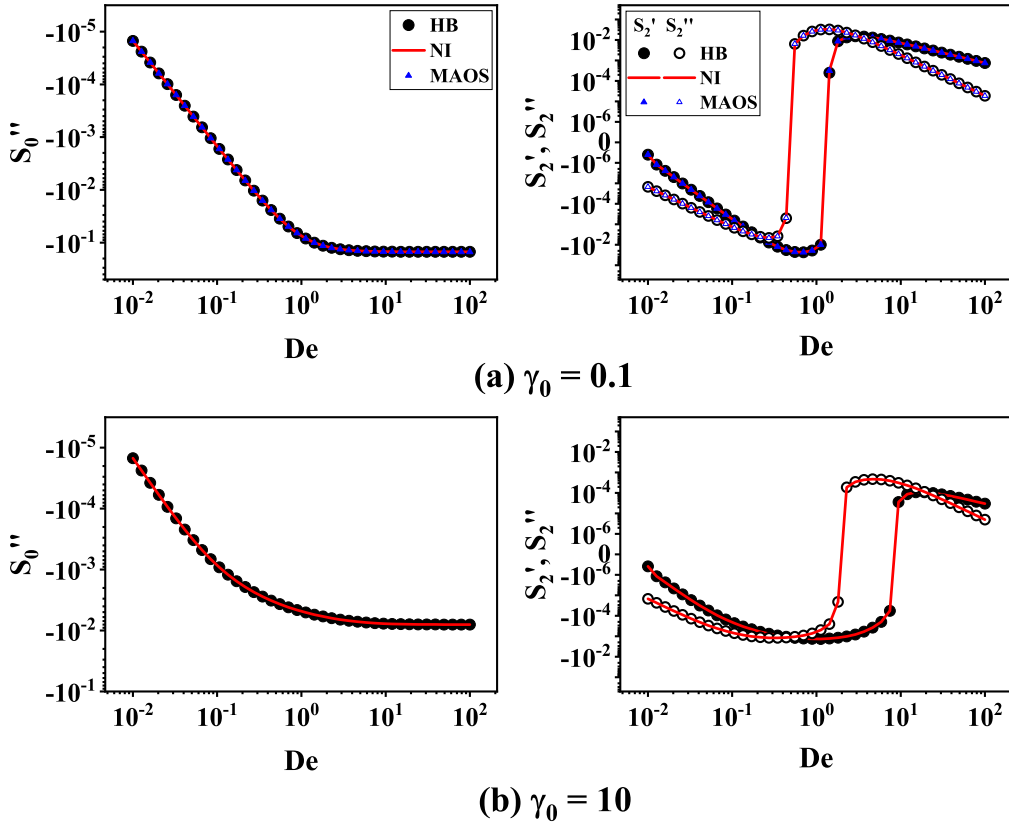


Figure 7: The Fourier coefficients of the second normal stress difference (S_0'' , S_2' , and S_2'') at (a) $\gamma_0 = 0.1$, and (b) $\gamma_0 = 0.01$ using harmonic balance (HB), and numerical integration (NI). The analytical MAOS solution is shown in subfigure (a).

which F_2'' , S_2' and S_2'' cross the x-axis shift to higher values with increasing γ_0 .

The results at $\gamma_0 = 0.1$ are in accordance with the analytical MAOS solution [15, 41]. In the linear regime, as the system moves from low-frequency viscous response to a high frequency elastic response, F_0'' and F_2'' plateau, which is expected since they are functions of G' , while F_2' peaks and then decreases due to its dependence on G'' . This can be understood in terms of MAOS relationships [15, 41], $F_0'' = G'(\omega)$, $F_2' = G''(\omega) - G''(2\omega)/2$, and $F_2'' = -G'(\omega) + G'(2\omega)/2$.

Interestingly, these relations also describe N_1 for the UCM model (eqn (2)), which is a special case of the Giesekus model with $\alpha = 0$ and $\eta_s = 0$. Thus, we may say that in the MAOS limit, where only ω , 2ω and 3ω terms are activated, G' , G'' , F_0'' , F_2' and F_2'' are not functions of α and behave essentially like a UCM fluid. However, the distinction between the Giesekus and UCM models becomes apparent from N_2 , which is zero for the UCM. For the Giesekus model, the Fourier coefficients of N_2 in the MAOS regime are non-zero and show a dependence on α . In addition, these coefficients S_0'' , S_2' and S_2'' cannot be expressed as a linear combination of G' and G'' , as opposed to F_0'' , F_2' and F_2'' . Thus, even in the linear regime, N_2 is a function of α and ω , while σ_{12} and N_1 are dependent only on ω . In principle, we can map a real system to a Giesekus model in the linear limit using N_2 to determine α . However, it is practically difficult since the signal is weak in this regime [41]. Thus, LAOS analysis of nonlinear stress waveforms is necessary to fit experimental data to the Giesekus model.

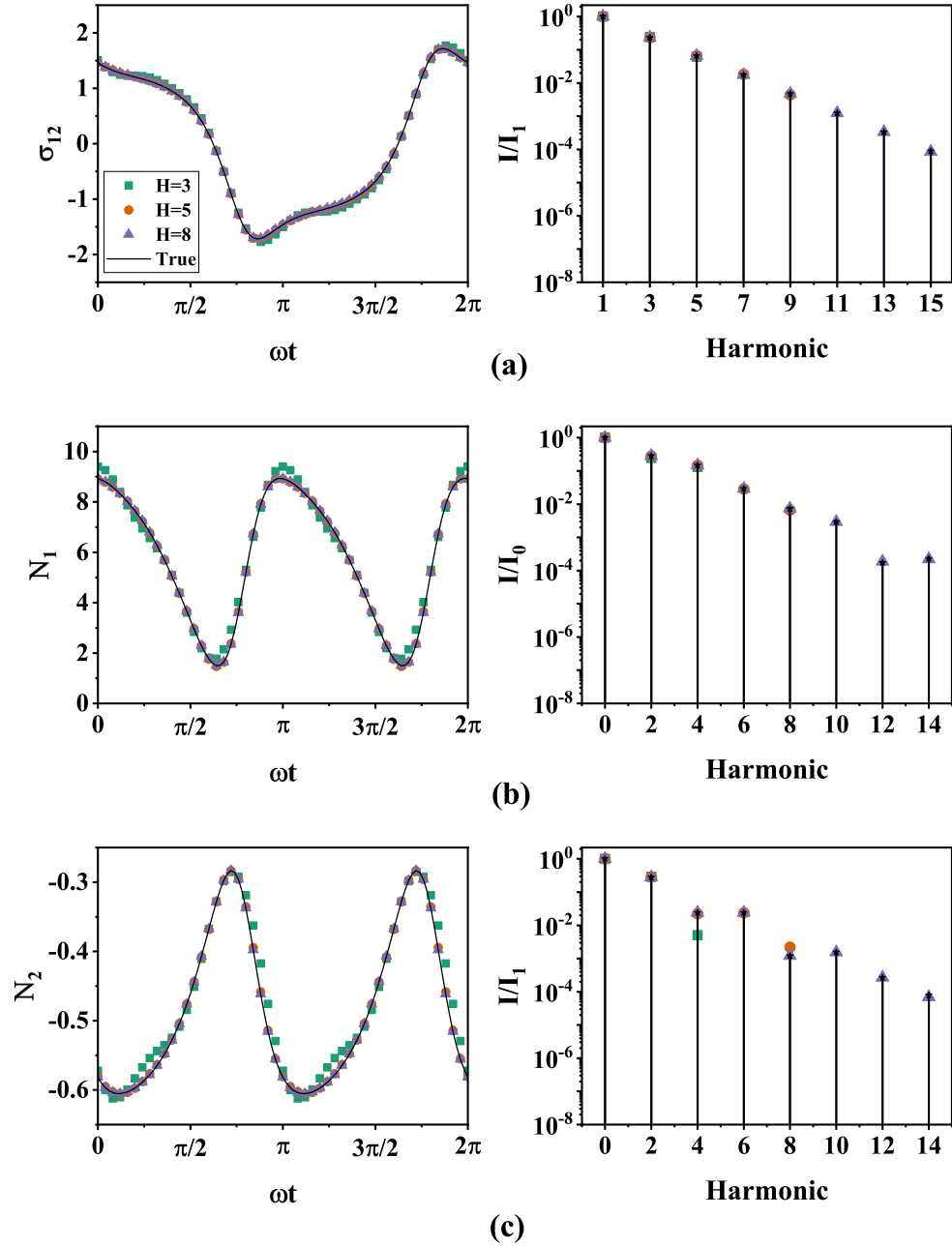


Figure 8: Stress waveforms and harmonic intensities for (a) σ_{12} , (b) N_1 and (c) N_2 at different H for $\gamma_0 = 10$ and $\omega = 1$ rad/s. The black solid lines (left) and stars (right) correspond to the true solution, while the symbols indicate results at different H .

3.3. Convergence and the number of harmonics

A parsimonious choice for the number of harmonics H ensures efficiency without compromising accuracy. Figures 8 and 9 show the stress waveforms and intensity plots for σ_{12} , N_1 and N_2 at $\gamma_0 = 10$ with $\omega = 1$ rad/s and $\omega = 100$ rad/s respectively, obtained using different values of H . The results are juxtaposed with the “true” solution to the Giesekus model equations which is approximated using a large number of harmonics, viz. $H = 30$. From previous results, we know that higher harmonics decay slowly at large Wi and moderate De . Therefore, selecting a large value for H improves accuracy as shown in figure 8. This impact is most pronounced in the second normal stress difference, figure 8(c). In figure 9 in contrast, where $\gamma_0 = 10$ and $De = 100$, higher harmonics decay rapidly, and increasing H does not significantly improve accuracy.

Regardless, the magnitudes of the individual harmonic intensities are relatively stable as H is increased. This provides a potential future pathway for systematically increasing the number of harmonics based on the decay characteristics of the harmonics, and level of accuracy desired. Such an adaptive protocol is not implemented in this study.

We now discuss the convergence of the HB method. Error bounds and convergence theorems for HB in different nonlinear vibration problems have already been established [78]. Here, we limit our discussion to harmonic convergence in systems that produce analytic outputs. Eqn. (29), which describes the pattern of convergence for such systems, can be adapted for

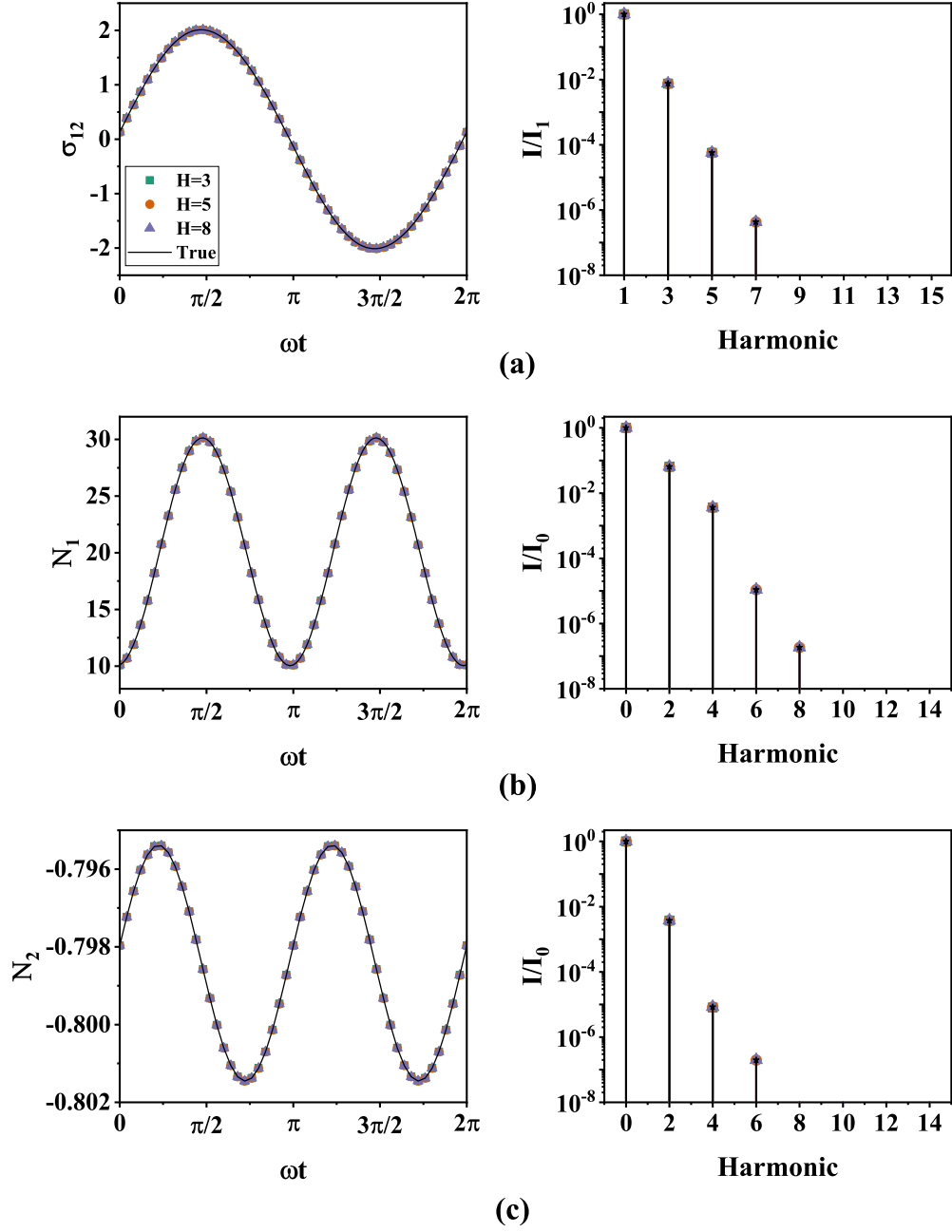


Figure 9: Stress waveforms and harmonic intensities for (a) σ_{12} , (b) N_1 and (c) N_2 at different H for $\gamma_0 = 10$ and $\omega = 100$ rad/s. The black solid lines (left) and stars (right) correspond to the true solution, while the symbols indicate results at different H .

our system using equations (35), (36) and (37) with $\mathbf{y} = [N_1, N_2, \sigma_{12}]^T$ and

$$\begin{aligned}\xi_F &= \|N_{1,H} - N_1(t)\|_\infty \leq u_F e^{-m_F(2H-2)}, \\ \xi_S &= \|N_{2,H} - N_2(t)\|_\infty \leq u_S e^{-m_S(2H-2)}, \\ \xi_G &= \|\sigma_{12,H} - \sigma_{12}(t)\|_\infty \leq u_G e^{-m_G(2H-1)},\end{aligned}\tag{44}$$

where $N_{1,H}$, $N_{2,H}$ and $\sigma_{12,H}$ are HB approximations to the true solutions N_1 , N_2 , and σ_{12} over a period of oscillation. The observed errors ξ_F , ξ_S , and ξ_G can be computed, and the decay coefficients m_F , m_S , and m_G can be empirically studied as a function of α , De, and Wi.

Figure 10 shows ξ_F and ξ_G plotted against $(2H - 1)$ and $(2H - 2)$, respectively, at $\gamma_0 = 10$ for four different frequencies. The empirically obtained error in all the plots shows an exponential decay to the true solution. We observe that convergence is most rapid at high ω , and most sluggish at intermediate ω . Interestingly, the decay coefficient m is almost the same for all three quantities i.e. $m_F \approx m_S \approx m_G$ as shown in figure 10(d).

We show the dependence of convergence rate on γ_0 in figure 11. As expected, the pace of convergence slows down with increasing γ_0 at a particular frequency. The value of m is inversely related to the extent of nonlinearity present in the system. The ‘‘U’’ shape of these curves indicates the linearity of the system at the low and high frequency ends despite being deep into the LAOS regime at large γ_0 .

3.4. Harmonic Balance vs Numerical Integration

In this section, we demonstrate the compelling value proposition of HB. It is both faster and more accurate than the standard NI technique. The solid lines in figures 5, 6, and 7 show the numerically integrated solution

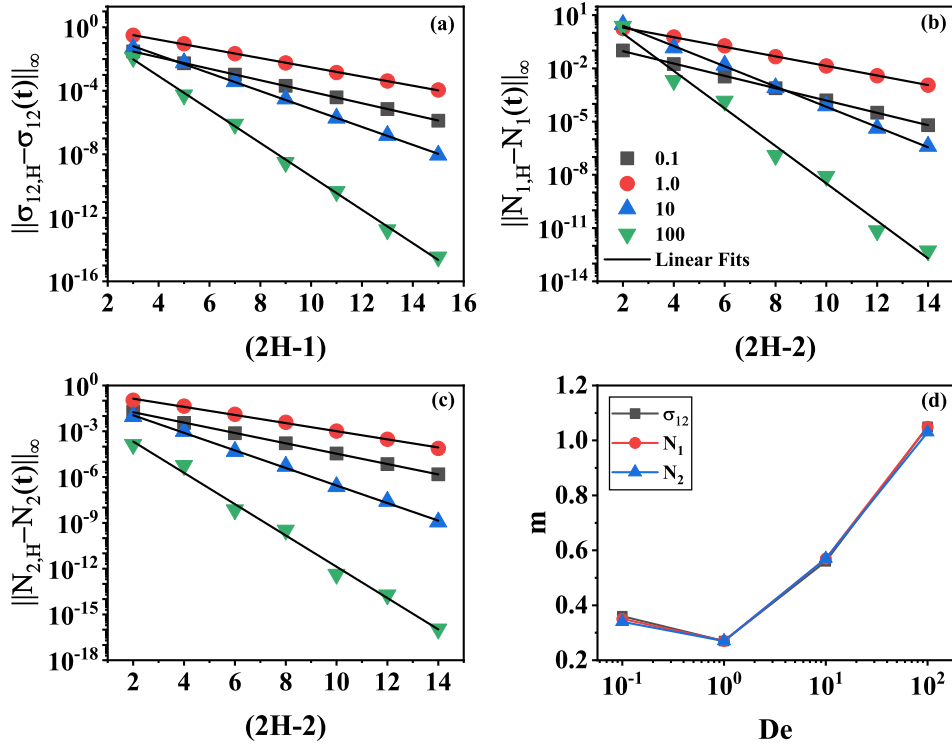


Figure 10: Convergence of the (a) shear stress, (b) first normal stress difference, and (c) second normal stress difference at different frequencies for $\gamma_0 = 10$, and (d) the corresponding exponential decay coefficient, m .

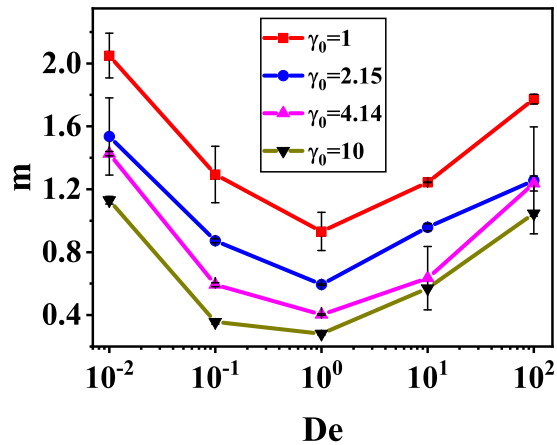


Figure 11: The convergence decay coefficient m at different strain amplitudes and frequencies.

to the IVP for the shear stress, first normal stress difference, and second normal stress difference respectively. Visually, the agreement between the harmonic coefficients obtained from both HB and numerical integration (NI) is excellent. Furthermore, the agreement between these numerical solutions and the analytical MAOS solution at $\gamma_0 = 0.1$ is also quite remarkable.

Figure 12 depicts the residual ϵ_r (eqn 43) at the two ends of the strain amplitude range, $\gamma_0 = 0.01$ and $\gamma_0 = 10$, for certain frequencies using both HB and NI. It is apparent from these plots that in terms of accuracy HB is superior to NI regardless of ω or γ_0 . At $\gamma_0 = 0.01$, only two harmonics ($H = 2$) are required to achieve an ϵ_r that is at least three orders of magnitude smaller than NI. Using a single additional harmonic term ($H = 3$) significantly improves the accuracy of HB at high frequencies at this γ_0 . It is apparent from figure 12(a) that increasing the number of harmonics any further does not improve the accuracy significantly. However, when γ_0 is increased to 10 in

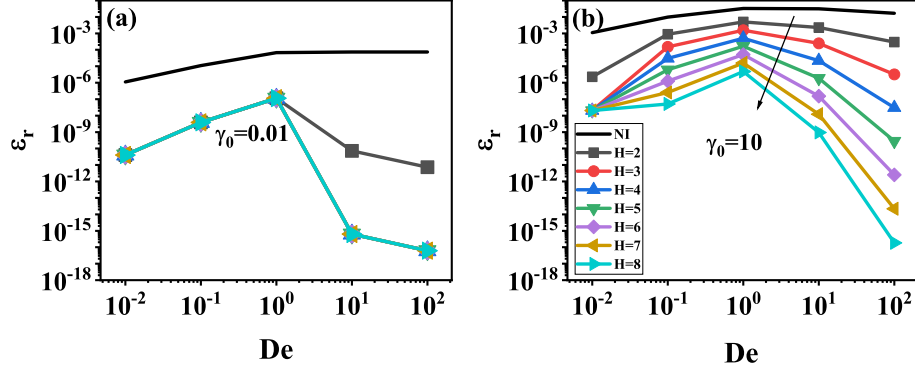


Figure 12: The residual ϵ_r (eqn 43) for HB and NI at (a) $\gamma_0 = 0.01$ and (b) $\gamma_0 = 10$.

figure 12(b), increasing H improves solution accuracy. However, even in this setting, HB with $H = 2$ harmonics outperforms NI in terms of accuracy.

However it is not fair to only compare accuracy without acknowledging the computational cost incurred in producing more accurate solutions. HB generates a system of $(6H - 2)$ nonlinear equations, which are evaluated at each iteration. Figure 13(a) shows the computation time on a standard laptop computer (Intel Xeon W-1290 CPU 3.2GHz) using HB for $\gamma_0 = 0.1$ and $\gamma_0 = 10$ at different frequencies. The number of equations, and the number of iterations required for convergence increase with H . The total computation time increases slightly faster than linearly with H . It also increases modestly with increasing ω .

On the other hand, the accuracy and computational cost of NI is dominated by the computation of the periodic steady state solution. Figure 13(b) compares the computational cost of NI and HB. NI takes roughly 10 – 100s depending on the frequency. In contrast, the computational cost of HB is at least three orders of magnitude lower as shown in Figure 13(b). Thus, HB is

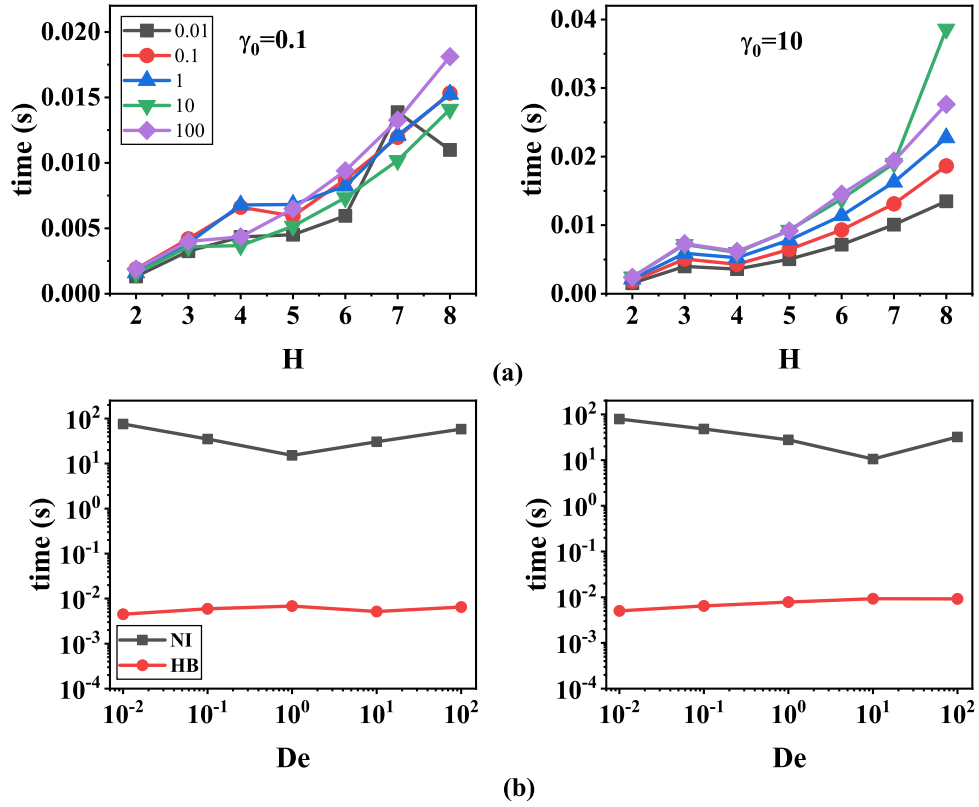


Figure 13: (a) The computation time for the HB method at different frequencies for $\gamma_0 = 0.1$ and $\gamma_0 = 10$. (b) Comparison of CPU time for the numerically integrated IVP and HB with $H = 5$ at different frequencies with $\gamma_0 = 0.1$ and $\gamma_0 = 10$.

superior to NI in terms of accuracy, as well as speed.

4. Conclusions and Perspective

In this work, HB is used to solve the Giesekus model under oscillatory shear. HB can be thought of as a numerical extension to the analytical approach of finding higher-order Fourier coefficients for constitutive models subjected to LAOS. It directly computes the periodic steady state solution by reducing a system of ODEs to a system of nonlinear equations, and avoids solving an IVP in the time domain. Numerical approximations converge exponentially to the true solution as the number of harmonics probed is increased. This enables fast and accurate estimation of higher-order Fourier coefficients. Due to its speed and accuracy, HB facilitates parameter estimation and model selection using a Bayesian framework that enables interpretation of LAOS data through the lens of constitutive theories.

The nonlinearity in the Giesekus model is quadratic. HB handles such nonlinearities elegantly as illustrated in this work. However, HB is not limited to the Giesekus model, and can accommodate a wide variety of nonlinear models using the alternating frequency-time (AFT) technique [78]. Ongoing work suggests that AFT enables generalization of HB to arbitrary differential constitutive equations. In the future, numerical path continuation techniques can also be used to explore stable and unstable solution branches.

Acknowledgements

This material is based partially upon work supported by the National Science Foundation under Grant No. DMR 1727870 (SS). Financial support

from the Science and Engineering Research Board, Government of India and Prime Minister Research Fellowship, Ministry of Education, Government of India is also acknowledged (YMJ and SM).

References

- [1] Y. Ma, D. Su, Y. Wang, D. Li, L. Wang, Effects of concentration and nacl on rheological behaviors of konjac glucomannan solution under large amplitude oscillatory shear (LAOS), *LWT* 128 (2020) 109466.
- [2] S. Khandavalli, J. P. Rothstein, Large amplitude oscillatory shear rheology of three different shear-thickening particle dispersions, *Rheol. Acta* 54 (7) (2015) 601–618.
- [3] R. W. Chan, Nonlinear viscoelastic characterization of human vocal fold tissues under large-amplitude oscillatory shear (LAOS), *J. Rheol.* 62 (3) (2018) 695–712.
- [4] P. Wapperom, A. Leygue, R. Keunings, P. Wapperom, A. Leygue, R. Keunings, Numerical simulation of large amplitude oscillatory shear of a high-density polyethylene melt using the MSF model, *J. Non-Newtonian Fluid Mech.* 130 (2) (2005) 63–76. doi : 10.1016/j.jnnfm.2005.08.002.
- [5] X. Li, S.-Q. Wang, X. Wang, Nonlinearity in large amplitude oscillatory shear (LAOS) of different viscoelastic materials, *J. Rheol.* 53 (5) (2009) 1255–1274.

- [6] C. J. Dimitriou, R. H. Ewoldt, G. H. McKinley, Describing and prescribing the constitutive response of yield stress fluids using large amplitude oscillatory shear stress (LAOStress), *J. Rheol.* 57 (1) (2013) 27–70.
- [7] J. Min Kim, A. P. Eberle, A. Kate Gurnon, L. Porcar, N. J. Wagner, The microstructure and rheology of a model, thixotropic nanoparticle gel under steady shear and large amplitude oscillatory shear (LAOS), *J. Rheol.* 58 (5) (2014) 1301–1328.
- [8] M. J. Armstrong, A. N. Beris, S. A. Rogers, N. J. Wagner, Dynamic shear rheology of a thixotropic suspension: Comparison of an improved structure-based model with large amplitude oscillatory shear experiments, *J. Rheol.* 60 (3) (2016) 433–450.
- [9] M. Armstrong, M. Scully, M. Clark, T. Corrigan, C. James, A simple approach for adding thixotropy to an elasto-visco-plastic rheological model to facilitate structural interrogation of human blood, *J. Non-Newtonian Fluid Mech.* 290 (2021) 104503. doi : 10.1016/j . j n n f m . 2021 . 104503.
- [10] G. J. Donley, J. R. de Bruyn, G. H. McKinley, S. A. Rogers, Time-resolved dynamics of the yielding transition in soft materials, *J. Non-Newtonian Fluid Mech.* 264 (2019) 117–134. doi : 10.1016/j . j n n f m . 2018 . 10 . 003.
- [11] R. H. Ewoldt, P. Winter, J. Maxey, G. H. McKinley, Large amplitude oscillatory shear of pseudoplastic and elastoviscoplastic materials, *Rheol. Acta* 49 (2) (2010) 191–212.

- [12] J. J. Stickel, J. S. Knutsen, M. W. Liberatore, Response of elastoviscoplastic materials to large amplitude oscillatory shear flow in the parallel-plate and cylindrical-couette geometries, *J. Rheol.* 57 (6) (2013) 1569–1596.
- [13] C. J. Dimitriou, L. Casanellas, T. J. Ober, G. H. McKinley, Rheo-piv of a shear-banding wormlike micellar solution under large amplitude oscillatory shear, *Rheol. Acta* 51 (5) (2012) 395–411.
- [14] T. B. Goudoulas, S. Pan, N. Germann, Nonlinearities and shear banding instability of polyacrylamide solutions under large amplitude oscillatory shear, *J. Rheol.* 61 (5) (2017) 1061–1083.
- [15] A. Kate Gurnon, N. J. Wagner, Large amplitude oscillatory shear (LAOS) measurements to obtain constitutive equation model parameters: Giesekus model of banding and nonbanding wormlike micelles, *J. Rheol.* 56 (2) (2012) 333–351.
- [16] R. Radhakrishnan, S. M. Fielding, Shear banding in large amplitude oscillatory shear (LAOS_{strain} and LAOS_{stress}) of soft glassy materials, *J. Rheol.* 62 (2) (2018) 559–576.
- [17] K. Atalık, R. Keunings, On the occurrence of even harmonics in the shear stress response of viscoelastic fluids in large amplitude oscillatory shear, *J. Non-Newtonian Fluid Mech.* 122 (1-3) (2004) 107–116.
- [18] K. Yang, W. Yu, Dynamic wall slip behavior of yield stress fluids under large amplitude oscillatory shear., *J. Rheol.* 61 (4) (2017) 627–641.

- [19] C. O. Klein, H. W. Spiess, A. Calin, C. Balan, M. Wilhelm, Separation of the nonlinear oscillatory response into a superposition of linear, strain hardening, strain softening, and wall slip response, *Macromolecules* 40 (12) (2007) 4250–4259.
- [20] M. D. Graham, Wall slip and the nonlinear dynamics of large amplitude oscillatory shear flows, *J. Rheol.* 39 (4) (1995) 697–712.
- [21] K. Suman, S. Shanbhag, Y. M. Joshi, Large amplitude oscillatory shear study of a colloidal gel at the critical state, arXiv preprint arXiv:2211.16724 (2022).
- [22] J. Kim, D. Merger, M. Wilhelm, M. E. Helgeson, Microstructure and nonlinear signatures of yielding in a heterogeneous colloidal gel under large amplitude oscillatory shear, *J. Rheol.* 58 (5) (2014) 1359–1390.
- [23] W.-x. Sun, L.-z. Huang, Y.-r. Yang, X.-x. Liu, Z. Tong, Large amplitude oscillatory shear studies on the strain-stiffening behavior of gelatin gels, *Chin. J. Polym. Sci.* 33 (1) (2015) 70–83.
- [24] T. S. Ng, G. H. McKinley, R. H. Ewoldt, Large amplitude oscillatory shear flow of gluten dough: A model power-law gel, *J. Rheol.* 55 (3) (2011) 627–654.
- [25] M. H. Wagner, V. H. Rolón-Garrido, K. Hyun, M. Wilhelm, Analysis of medium amplitude oscillatory shear data of entangled linear and model comb polymers, *J. Rheol.* 55 (3) (2011) 495–516.
- [26] K. Hyun, E. S. Baik, K. H. Ahn, S. J. Lee, M. Sugimoto, K. Koyama, Fourier-transform rheology under medium amplitude oscillatory shear

- for linear and branched polymer melts, *J. Rheol.* 51 (6) (2007) 1319–1342.
- [27] D. Hoyle, D. Auhl, O. Harlen, V. Barroso, M. Wilhelm, T. McLeish, Large amplitude oscillatory shear and fourier transform rheology analysis of branched polymer melts, *J. Rheol.* 58 (4) (2014) 969–997.
- [28] K. S. Cho, K.-W. Song, G.-S. Chang, Scaling relations in nonlinear viscoelastic behavior of aqueous pco solutions under large amplitude oscillatory shear flow, *Journal of Rheology* 54 (1) (2010) 27–63. doi : 10.1122/1.3258278.
- [29] K. S. Cho, J. W. Kim, J.-E. Bae, J. H. Youk, H. J. Jeon, K.-W. Song, Effect of temporary network structure on linear and nonlinear viscoelasticity of polymer solutions, *Korea-Aust. Rheol. J.* 27 (2) (2015) 151–161. doi : 10.1007/s13367-015-0015-y.
- [30] K. S. Cho, *Viscoelasticity of Polymers: Theory and Numerical Algorithms*, Springer, Dordrecht, the Netherlands, 2016.
- [31] I. F. MacDonald, B. D. Marsh, E. Ashare, Rheological behavior for large amplitude oscillatory motion, *Chem. Eng. Sci.* 24 (10) (1969) 1615–1625.
- [32] D. S. Pearson, W. E. Rochefort, Behavior of concentrated polystyrene solutions in large-amplitude oscillating shear fields, *J. Polym. Sci. Polym. Phys.* 20 (1) (1982) 83–98.
- [33] A. J. Giacomin, C. Saengow, M. Guay, C. Kolutawong, Padé approximants for large-amplitude oscillatory shear flow, *Rheol. Acta* 54 (8) (2015) 679–693.

- [34] R. H. Ewoldt, A. Hosoi, G. H. McKinley, New measures for characterizing nonlinear viscoelasticity in large amplitude oscillatory shear, *J. Rheol.* 52 (6) (2008) 1427–1458.
- [35] K. S. Cho, K. Hyun, K. H. Ahn, S. J. Lee, A geometrical interpretation of large amplitude oscillatory shear response, *J. Rheol.* 49 (3) (2005) 747–758.
- [36] J.-E. Bae, K. S. Cho, Analytical studies on the LAOS behaviors of some popularly used viscoelastic constitutive equations with a new insight on stress decomposition of normal stresses, *Phys. Fluids* 29 (9) (2017) 093103. doi : 10. 1063/1. 5001742.
- [37] K. Hyun, M. Wilhelm, Establishing a new mechanical nonlinear coefficient q from ft-rheology: First investigation of entangled linear and comb polymer model systems, *Macromolecules* 42 (1) (2009) 411–422.
- [38] S. A. Rogers, M. P. Lettinga, A sequence of physical processes determined and quantified in large-amplitude oscillatory shear (LAOS): Application to theoretical nonlinear models, *J Rheol* 56 (1) (2012) 1–25.
- [39] J. D. Ferry, *Viscoelastic properties of polymers*, 3rd Edition, John Wiley & Sons, New York, NY, 1980.
- [40] A. J. Giacomin, J. M. Dealy, Large-amplitude oscillatory shear, in: A. A. Collyer (Ed.), *Techniques in Rheological Measurement*, Springer Netherlands, Dordrecht, 1993, pp. 99–121.
- [41] J. G. Nam, K. Hyun, K. H. Ahn, S. J. Lee, Prediction of normal stresses

- under large amplitude oscillatory shear flow, *J. Non-Newtonian Fluid Mech.* 150 (1) (2008) 1–10.
- [42] S. Shanbhag, Y. M. Joshi, Kramers–kronig relations for nonlinear rheology. part i: General expression and implications, *J. Rheol.* 66 (5) (2022) 973–982.
- [43] S. Shanbhag, Y. M. Joshi, Kramers–kronig relations for nonlinear rheology. part ii: Validation of medium amplitude oscillatory shear (maos) measurements, *J. Rheol.* 66 (5) (2022) 925–936.
- [44] C. Saengow, A. J. Giacomin, C. Kolutawong, Exact analytical solution for large-amplitude oscillatory shear flow, *Macromol. Theory Simul.* 24 (4) (2015) 352–392.
- [45] P. Pongthong, A. Giacomin, C. Saengow, C. Kolutawong, Exact solution for intrinsic nonlinearity in oscillatory shear from the corotational maxwell fluid, *J. Non-Newtonian Fluid Mech.* 265 (2019) 53–65. doi : 10.1016/j.jnnfm.2019.01.001.
- [46] C. Saengow, A. J. Giacomin, C. Kolutawong, Exact analytical solution for large-amplitude oscillatory shear flow from oldroyd 8-constant framework: Shear stress, *Phys. Fluids* 29 (4) (2017) 043101.
- [47] C. Saengow, A. J. Giacomin, Normal stress differences from oldroyd 8-constant framework: Exact analytical solution for large-amplitude oscillatory shear flow, *Phys. Fluids* 29 (12) (2017) 121601.
- [48] E. Helfand, D. S. Pearson, Calculation of the nonlinear stress of polymers

- in oscillatory shear fields, *J. Polym. Sci. Polym. Phys.* 20 (7) (1982) 1249–1258.
- [49] N. A. Bharadwaj, R. H. Ewoldt, Constitutive model fingerprints in medium-amplitude oscillatory shear, *J. Rheol.* 59 (2) (2015) 557–592.
- [50] R. Bird, A. Giacomin, A. Schmalzer, C. Aumnate, Dilute rigid dumbbell suspensions in large-amplitude oscillatory shear flow: Shear stress response, *J. Chem. Phys.* 140 (7) (2014) 074904.
- [51] X.-J. Fan, R. B. Bird, A kinetic theory for polymer melts vi. calculation of additional material functions, *J. Non-Newtonian Fluid Mech.* 15 (3) (1984) 341–373.
- [52] N. A. Bharadwaj, R. H. Ewoldt, The general low-frequency prediction for asymptotically nonlinear material functions in oscillatory shear, *J. Rheol.* 58 (4) (2014) 891–910.
- [53] W. Yu, M. Bousmina, M. Grmela, C. Zhou, Modeling of oscillatory shear flow of emulsions under small and large deformation fields, *J. Rheol.* 46 (6) (2002) 1401–1418.
- [54] L. Martinetti, R. H. Ewoldt, Time-strain separability in medium-amplitude oscillatory shear, *Phys. Fluids* 31 (2) (2019) 021213.
- [55] S. Shanbhag, S. Mittal, Y. M. Joshi, Spectral method for time-strain separable integral constitutive models in oscillatory shear, *Phys. Fluids* 33 (11) (2021) 113104.

- [56] S. Shanbhag, Analytical rheology of blends of linear and star polymers using a Bayesian formulation, *Rheol. Acta* 49 (4) (2010) 411–422.
- [57] A. Takeh, J. Worch, S. Shanbhag, Analytical rheology of metallocene-catalyzed polyethylenes, *Macromolecules* 44 (9) (2011) 3656–3665. doi : 10.1021/ma2004772.
- [58] H. Giesekus, A simple constitutive equation for polymer fluids based on the concept of deformation-dependent tensorial mobility, *J. Non-Newtonian Fluid Mech.* 11 (1-2) (1982) 69–109.
- [59] J. Yoo, H. C. Choi, On the steady simple shear flows of the one-mode Giesekus fluid, *Rheol. Acta* 28 (1) (1989) 13–24.
- [60] G. Schleiniger, R. Weinacht, A remark on the Giesekus viscoelastic fluid, *J. Rheol.* 35 (6) (1991) 1157–1170.
- [61] M. Yao, G. H. McKinley, B. Debbaut, Extensional deformation, stress relaxation and necking failure of viscoelastic filaments, *J. Non-Newtonian Fluid Mech.* 79 (2-3) (1998) 469–501.
- [62] T. Holz, P. Fischer, H. Rehage, Shear relaxation in the nonlinear-viscoelastic regime of a Giesekus fluid, *J. Non-Newtonian Fluid Mech.* 88 (1-2) (1999) 133–148.
- [63] P. Fischer, H. Rehage, Non-linear flow properties of viscoelastic surfactant solutions, *Rheol. Acta* 36 (1) (1997) 13–27.
- [64] H. Rehage, R. Fuchs, Experimental and numerical investigations of the non-linear rheological properties of viscoelastic surfactant solutions: ap-

- plication and failing of the one-mode Giesekus model, *Colloid Polym. Sci.* 293 (11) (2015) 3249–3265.
- [65] R. Bandyopadhyay, A. Sood, Effect of silica colloids on the rheology of viscoelastic gels formed by the surfactant cetyl trimethylammonium tosylate, *J. Colloid Interface Sci.* 283 (2) (2005) 585–591.
- [66] J. Kokini, M. Dhanasekharan, C. Wang, H. Huang, Integral and differential linear and non-linear constitutive models for rheology of wheat flour doughs, Technomics Publishing Co. Inc., Lancaster, PA, 2000.
- [67] M. Dhanasekharan, C. Wang, J. Kokini, Use of nonlinear differential viscoelastic models to predict the rheological properties of gluten dough, *J. Food Process Eng* 24 (3) (2001) 193–216.
- [68] O. C. Duvarci, G. Yazar, J. L. Kokini, The SAOS, MAOS and LAOS behavior of a concentrated suspension of tomato paste and its prediction using the Bird-Carreau (SAOS) and Giesekus models (MAOS-LAOS), *J. Food Eng.* 208 (2017) 77–88.
- [69] A. Calin, M. Wilhelm, C. Balan, Determination of the non-linear parameter (mobility factor) of the Giesekus constitutive model using LAOS procedure, *J. Non-Newtonian Fluid Mech.* 165 (23-24) (2010) 1564–1577.
- [70] L. Quinzani, G. McKinley, R. Brown, R. Armstrong, Modeling the rheology of polyisobutylene solutions, *J. Rheol.* 34 (5) (1990) 705–748.
- [71] B. Debbaut, H. Burhin, Large amplitude oscillatory shear and fourier-transform rheology for a high-density polyethylene: Experiments and numerical simulation, *J. Rheol.* 46 (5) (2002) 1155–1176.

- [72] A. Öztekin, R. A. Brown, G. H. McKinley, Quantitative prediction of the viscoelastic instability in cone-and-plate flow of a Boger fluid using a multi-mode Giesekus model, *J. Non-Newtonian Fluid Mech.* 54 (1994) 351–377.
- [73] K. Atalık, R. Keunings, Non-linear temporal stability analysis of viscoelastic plane channel flows using a fully-spectral method, *J. Non-Newtonian Fluid Mech.* 102 (2) (2002) 299–319. doi : 10.1016/S0377-0257(01)00184-7.
- [74] D. Borzacchiello, E. Abisset-Chavanne, F. Chinesta, R. Keunings, Orientation kinematics of short fibres in a second-order viscoelastic fluid, *Rheol. Acta* 55 (5) (2016) 397–409. doi : 10.1007/s00397-016-0929-4.
- [75] R. H. Ewoldt, G. H. McKinley, On secondary loops in LAOS via self-intersection of lissajous–bowditch curves, *Rheol. Acta* 49 (2) (2010) 213–219.
- [76] J.-E. Bae, K. S. Cho, Semianalytical methods for the determination of the nonlinear parameter of nonlinear viscoelastic constitutive equations from LAOS data, *J. Rheol.* 59 (2) (2015) 525–555.
- [77] K. Atkinson, W. Han, D. E. Stewart, *Numerical Solution of Ordinary Differential Equations*, John Wiley & Sons, Ltd, Hoboken, New Jersey, 2009. doi : <https://doi.org/10.1002/9781118164495>.
- [78] M. Krack, J. Gross, *Harmonic Balance for Nonlinear Vibration Problems*, Springer International Publishing, Cham, 2019. doi : 10.1007/978-3-030-14023-6.

- [79] A. S. Khair, Large amplitude oscillatory shear of the giesekus model, *J. Rheol.* 60 (2) (2016) 257–266. doi : 10.1122/1.4941423.
- [80] R. S. Jeyaseelan, A. J. Giacomin, Network theory for polymer solutions in large amplitude oscillatory shear, *J. Non-Newtonian Fluid Mech.* 148 (1-3) (2008) 24–32.
- [81] T.-T. Tee, J. Dealy, Nonlinear viscoelasticity of polymer melts, *Trans. Soc. Rheol.* 19 (4) (1975) 595–615.
- [82] S. Khandavalli, J. Hendricks, C. Clasen, J. P. Rothstein, A comparison of linear and branched wormlike micelles using large amplitude oscillatory shear and orthogonal superposition rheology, *J. Rheol.* 60 (6) (2016) 1331–1346.
- [83] A. A. Moud, M. Kamkar, A. Sanati-Nezhad, S. H. Hejazi, U. Sundararaj, Viscoelastic properties of poly (vinyl alcohol) hydrogels with cellulose nanocrystals fabricated through sodium chloride addition: Rheological evidence of double network formation, *Colloids Surf., A* 609 (2021) 125577.
- [84] G. Yazar, O. Duvarci, S. Tavman, J. L. Kokini, Non-linear rheological behavior of gluten-free flour doughs and correlations of LAOS parameters with gluten-free bread properties, *J. Cereal Sci.* 74 (2017) 28–36.
- [85] S. Yasin, M. Hussain, Q. Zheng, Y. Song, Large amplitude oscillatory rheology of silica and cellulose nanocrystals filled natural rubber compounds, *J. Colloid Interface Sci.* 588 (2021) 602–610.

- [86] A. Leygue, C. Bailly, R. Keunings, A tube-based constitutive equation for polydisperse entangled linear polymers, *J. Non-Newtonian Fluid Mech.* 136 (1) (2006) 1–16.
- [87] K. Hyun, W. Kim, S. Joon Park, M. Wilhelm, Numerical simulation results of the nonlinear coefficient Q from FT-rheology using a single mode pom-pom model, *J. Rheol.* 57 (1) (2013) 1–25.